Biological Sciences: Cell Biology

Regulation of INF2-mediated actin polymerization through site-specific lysine acetylation of actin itself

Mu A[1], Tak Shun Fung[1], Lisa M. Francomacaro[1], Thao Huynh[1], Tommi Kotila[2], Zdenek Svindrych[1] & Henry N. Higgs[1]*

[1]Department of Biochemistry and Cell Biology, Geisel School of Medicine at Dartmouth, Hanover NH 03755
[2]HiLIFE Institute of Biotechnology, University of Helsinki, Finland

*Corresponding author (henry.higgs@dartmouth.edu; 1-603-650-1520)

Keywords: cyclase-associated protein, WH2 motif, nucleation, U2OS cells

Abstract

INF2 is a formin protein that accelerates actin polymerization. A common mechanism for formin regulation is autoinhibition, through interaction between the N-terminal diaphanous inhibitory domain (DID) and C-terminal diaphanous autoregulatory domain (DAD). We recently showed that INF2 utilizes a variant of this mechanism which we termed 'facilitated autoinhibition', whereby a complex consisting of cyclase-associated protein (CAP) bound to lysine-acetylated actin (KAc-actin) is required for INF2 inhibition, in a manner requiring INF2-DID. De-acetylation of actin in the CAP/KAc-actin complex activates INF2. Here, we use lysine-to-glutamine mutations as acetyl-mimetics to map the relevant lysines on actin for INF2 regulation, focusing on K50, K61 and K328. Biochemically, K50Q- and K61Q-actin, when bound to CAP2, inhibit full-length INF2 but not INF2 lacking DID. When not bound to CAP, these mutant actins polymerize similarly to WT-actin in the presence and absence of INF2, suggesting that the effect of the mutation is directly on INF2 regulation. In U2OS cells, K50Q- and K61Q-actin inhibit INF2-mediated actin polymerization when expressed at low levels. Direct binding studies show that the CAP WH2 domain binds INF2-DID with sub-micromolar affinity but has weak affinity for actin monomers, while INF2-DAD binds CAP/K50Q-actin 5-fold better than CAP/WT-actin. Actin in complex with full-length CAP2 is predominately ATP-bound. These interactions suggest an inhibition model whereby CAP/KAc-actin serves as a bridge between INF2 DID and DAD. In U2OS cells, INF2 is 90 and 5-fold less abundant than CAP1 and CAP2, respectively, suggesting that there is sufficient CAP for full INF2 inhibition.

Significance Statement

Tight regulation is required to control biochemical reactions in cells, so that these reactions can be activated precisely when and where needed. Our work focuses on actin, a protein that polymerizes into filaments in at least 20 distinct processes in mammalian cells. We have previously shown that a relatively minor modification on actin, lysine acetylation, is crucial for regulation of a specific population of actin filaments, through a protein called INF2. Here, we identify key acetylated lysines that control INF2 activity. INF2 mutations link to two human diseases, focal segmental glomerulosclerosis (a kidney disease) and Charcot-Marie-Tooth disease (a neuropathy), and our findings further the mechanistic understanding of these diseases.

Introduction

A common mechanism for protein regulation is autoinhibition, whereby intra-molecular contacts inhibit the protein's biological function. Formin proteins are actin assembly factors. Several of the 15 mammalian formins are autoinhibited through interaction between the N-terminal diaphanous inhibitory domain (DID) and the C-terminal diaphanous autoregulatory domain (DAD), which blocks the ability of the formin homology 2 (FH2) domain to accelerate actin polymerization (1, 2). One formin, INF2, employs a variation of this mechanism. Despite having both DID and DAD sequences which are necessary for INF2 regulation in cells (Figure 1A), purified INF2 is fully active in biochemical assays. Direct binding studies show that INF2's DID/DAD interaction is at least 10-fold weaker than that of mDia1 (3, 4), providing an explanation for the lack of autoinhibition. In addition, INF2's DAD is similar to an actin-binding WH2 motif (5), and binds actin monomers with high affinity (6, 7). These findings led us to predict that an additional protein is required to inhibit INF2 in a DID/DAD-dependent manner.

We isolated a protein complex capable of inhibiting purified INF2 in a manner that requires INF2's DID (8). The complex consists of cyclase-associated protein (CAP) bound to actin itself. Both mammalian CAP proteins, CAP1 and CAP2, can inhibit INF2. CAP consists of an N-terminal region containing an oligomerization domain (OD) and a helical folded domain (HFD), a middle region consisting of a WH2 motif flanked by proline-rich sequences, and a C-terminal CARP domain (Figure 1B). The N-terminal OD from both budding yeast CAP and human CAP1 has been shown to hexamerize (9, 10), which is consistent with our results on full-length CAP2 (8). Two regions of CAP can bind actin monomers: the WH2 motif and the CARP domain. The CARP domain binds ADP-actin with high affinity, while the WH2 domain binds ATP-actin with lower affinity (11-13). A structure of CARP/actin complex shows that dimeric CARP binds two actin monomers in a manner that exposes actin's WH2 binding site (12)(Figure 1C). CAP has multiple potential functions in actin dynamics, including acceleration of actin nucleotide exchange and enhancing cofilin-mediated depolymerization (14). This latter function requires the HFD, that can bind cofilin-actin complex (15-18).

A key feature of INF2 inhibition by CAP/actin complex is that lysine acetylation of the actin is required, as supported by the following findings (8). First, pre-treatment of CAP/actin with histone deacetylase 6 (HDAC6) virtually eliminates INF2 inhibition. Second, isolation of CAP/actin complex from mammalian cells treated with HDAC6 inhibitor increases both the amount of acetylated actin bound to CAP and the inhibitory potency of the CAP/actin complex. Third, transient activation of INF2 in cells causes a decrease in lysine-acetylated actin in CAP/actin complex on a similar time course to INF2 activation. Fourth, HDAC6 inhibition blocks INF2-mediated actin polymerization in cells.

Lysine acetylation of histones and other nuclear proteins has long been known to serve as an important regulatory mechanism for gene expression, but multiple cytoplasmic proteins are also known to be lysine-acetylated (19, 20), including tubulin, cortactin, and the formin mDia2 (21-23). Actin itself can be acetylated on multiple lysines (24, 25). The functional significance of actin acetylation has not been studied extensively, with one published study suggesting that

acetylation of K326 or K328 in *Drosophila* flight muscle causes defects in morphology and performance (26).

We address two questions in the current work. First, which lysine(s) on actin is/are relevant for acetylation-mediated INF2 regulation? Using lysine-to-glutamine mutations to mimic acetylation, we find that K50 and K61 are key residues whereas K328 is not. Second, what interactions between CAP, lysine-acetylated actin (KAc-actin) and INF2 mediate the inhibitory interaction? Two proposed mechanisms (8) are: 1) 'facilitated autoinhibition', whereby CAP/KAc-actin binds the DID/DAD complex to secure the low-affinity DID/DAD interaction; or 2) the 'bridge' model, whereby CAP/KAc-actin binds between the DID and the DAD. Our studies here provide support for the bridge model (Figure 1D).

Results

K-to-Q mutants of β-actin retain similar polymerization properties to WT-actin

We reasoned that lysine-to-glutamine mutations might functionally mimic acetylation at specific sites on actin. Similar mutations have been used to mimic acetylation of actin (26) and other proteins (27-29). Here, we examine three mutants to human β-actin biochemically and in cells: K50Q, K61Q, and K328Q. These residues are surface-exposed in the filament structure, with K50 and K61 being in sub-domain 2, and K328 in sub-domain 3.

To produce β-actin amenable for biochemical tests, we used a system similar to those used previously (30, 31), in which actin is expressed as an N-terminal fusion with the monomer-binding protein thymosin β4 (Tβ4), then cleaved with chymotrypsin post-purification, resulting in actin with no additional amino acids. The initial affinity purification step results in actin-Tβ4 without detectable free actin (SI Appendix Fig. S1A), suggesting that no endogenous actin co-purifies. Use of this system results in actin without other major protein bands for WT, K50Q, K61Q and K328Q (SI Appendix Fig. S1B).

Next, we conducted tests to assess the functionality of the recombinant actins, compared to rabbit muscle (RSK) actin. All recombinant actins are polymerization-competent. By high-speed pelleting assay (32), less than 0.17 μM actin is in the supernatant after overnight polymerization (Fig. 2A, SI Appendix Fig. S1C), suggesting that the critical concentrations are similar to RSK-actin (33). By pyrene-actin polymerization, all actins polymerize with similar kinetics (Fig. 2B), with two variations. First, WT β-actin has a shorter polymerization lag than either RSK- actin or any of the mutants. Second, the plateau fluorescence for all mutant actins is approximately 10% lower than for WT β-actin or RSK- actin. This difference in plateau likely represents a difference in pyrene fluorescence change rather than a difference in polymerization ability, given the similar critical concentrations. We quantified polymerization rates of the actins by determining the time to ½ maximum polymerization (Fig. 2D), and found that the rates of WT, K61Q and K328Q β-actin are faster than RSK-actin, whereas K50Q β-actin is indistinguishable from RSK-actin.

We also assessed the effects of INF2 on the polymerization of recombinant actins, testing both full-length INF2 and INF2-FFC. The INF2 isoform used in this study is the nonCAAX variant, which is largely cytosolic and lacks the C-terminal prenylation site of the INF2-CAAX isoform (34, 35). By high-speed pelleting assay, both INF2 constructs cause a slight increase in the actin recovered in the supernatant (Fig. 2A, SI Appendix Fig. S1C), suggestive of a shift in critical concentration due to INF2's effects on barbed end dynamics (36, 37). The degree of this shift is similar for all actins tested, and is below 0.2 μM. As a control, all actin's polymerized in the presence of barbed end capping protein results in a shift in supernatant actin to a value similar to the pointed end critical concentration (Fig. 2A, SI Appendix Fig. S1C), suggesting that capping protein interaction is not fundamentally affected by the mutations.

By pyrene-actin assay in the presence of INF2-FFC or INF2-FL, all three actin mutants display a lower polymerization plateau than WT β-actin or RSK-actin (Fig. 2C, SI Appendix Fig. S1D). This

effect is similar to that found for actin alone, again suggesting a change in pyrene-actin fluorescence rather than in polymerization properties. In terms of polymerization rate, the values for all mutants in the presence of INF2-FL are slightly slower than for WT β-actin or for RSK actin (Fig. 2D).

In summary, these analyses suggest that the β-actins produced recombinantly have largely similar polymerization properties to RSK-actin, both in the absence and presence of INF2. The minor differences in their polymerization rates in the presence of INF2-FL do not account for the effects of specific mutants on INF2-FL activity when in complex with CAP2, described next.

K50Q and K61Q actin are INF2 inhibitors when in complex with CAP2

We assessed the ability of CAP-complexed β-actin mutants to inhibit actin polymerization by INF2-FL. Previously, we found that purified CAP1 or CAP2 preparations from HEK293 cells, containing approximately equi-molar actin, were poor INF2 inhibitors. However, CAP became a potent INF2 inhibitor when the bound actin (293A) was exchanged with certain types of actin (mouse brain or chicken skeletal muscle actin), but not with others (RSK-actin) (8). Here, we used a similar approach to exchange WT- or K-to-Q β-actin mutants onto CAP2.

Exchange of CAP2/293A with either RSK-actin or any of the recombinantly-expressed β-actins results in similar CAP/actin ratios (SI Appendix Fig. S2A). We also examined the nucleotide state of the bound actin before and after exchange. Purified CAP2/actin contains both ATP and ADP, with ATP being ~65% of the total (SI Appendix Fig. S2B). Interestingly, the 'mock' exchange reaction, in which CAP2/actin is incubated with buffer containing 0.2 mM ATP, causes the ATP:ADP ratio to increase, suggesting nucleotide exchange on the bound actin. Exchange with either WT- or K50Q-actin results in a similar increase in ATP:ADP ratio (Fig. S2C).

We assessed the effects of exchanged CAP2/actin complexes on actin polymerization by full-length INF2-nonCAAX in pyrene-actin assays. At 1 μM CAP, the CAP/K50Q and CAP/K61Q complexes display strong inhibition of INF2 activity (Fig. 3A). In contrast, the CAP/K328Q, CAP/WT, CAP/RSK, and CAP/293A complexes display much less inhibition. Concentration curves show that CAP/K50Q has an IC_{50} of 212 nM, while CAP/K61Q has an approximate IC_{50} of 770 nM and does not reach an inhibition plateau at the highest concentration tested (Fig. 3B). The other constructs display minimal inhibition at all concentrations tested (Fig. 3B).

We tested the specificity of this CAP/actin inhibition for full-length INF2 in two ways. First, we examined the effects of the CAP/actin complexes on polymerization of actin alone. At 1 μM CAP, all complexes slightly accelerate actin polymerization (Fig. 3C), similar to our past results on CAP/actin complexes (8). Next, we examined the effects of CAP/actin complexes on actin polymerization acceleration by INF2-FFC, which lacks the N-terminal DID (Fig. 1A). At 1 μM CAP, none of the complexes affect INF2-FFC activity (Fig. 3D).

Finally, we asked whether increasing the percentage of K50Q-actin to WT-actin in the CAP/actin complex caused a progressive change in INF2 inhibition, by altering the K50Q:WT ratio in

exchange reactions. Increasing the K50Q:WT percentage causes a progressive increase in INF2 inhibition (Fig. 3E, F). Since the amount of actin bound to CAP is not different between K50Q- and WT-actin exchanged CAP (Fig. S2A), this suggests that an increased proportion of Ac-actin bound to CAP increases inhibitory potency.

These results suggest that the K50Q and K61Q actin mutants, when complexed with CAP2, act as potent inhibitors of INF2 activity, presumably by acting as acetylation mimics. This inhibition requires INF2's DID, suggesting that the CAP/actin complexes aid INF2 auto-inhibition. In contrast, the K328Q mutant is a poor actin inhibitor.

We also tried to load a previously described C-terminal construct of CAP1 (15), containing the WH2 motif and CARP domain, with ATP-actin. Interestingly, while full-length CAP2 can remain stably bound to ATP-actin, we only obtain ~15% binding of ATP-actin to CAP1-Cterm, for RSK-actin, WT-, or K50Q-β-actin (SI Appendix Fig. S2D). This result agrees with past studies showing low affinity of this construct for ATP-actin (15).

Acetyl-mimetic actin mutants inhibit INF2-mediated actin polymerization in cells

To test the effect of K-to-Q mutant actins in cells, we constructed a bis-cistronic vector co-expressing untagged β-actin along with mCherry (Fig. 4A). We transiently transfected this actin/mCherry vector into U2OS cells, along with a vector expressing GFP-F-tractin, an actin filament probe. We then assessed cytosolic actin filament levels induced by ionomycin stimulation, which we and others have previously shown to be INF2-dependent (38-41). We image the cells in a medial z-section, to avoid abundant basal actin structures. In control cells without the actin/mCherry vector or expressing mCherry alone, ionomycin causes a transient increase in cytoplasmic actin filaments, as detected by an increase in filamentous GFP-Ftractin (SI Appendix Fig. S3A,B). Cells expressing WT- or K328Q-actin display a similar ionomycin-induced actin burst (Fig. 4B,C). In contrast, cells expressing the K50Q or K61Q mutants display greatly reduced responses to ionomycin (Fig. 4B,C). These results suggest that acetylation at K50 or K61 is sufficient for potent INF2 inhibition in cells.

To test whether the actin mutants affect other types of stimulus-induced actin polymerization, we examined U2OS response to the mitochondrial un-coupler CCCP, which induces a rapid and transient actin polymerization burst around mitochondria that is INF2-independent (42). Expression of either WT-actin or K50Q-actin construct in U2OS cells does not affect the CCCP-induced actin burst (Fig. 4D, SI Appendix Fig. S3C). This result suggests that the effect of the K50Q mutant on ionomycin-induced actin polymerization is INF2-specific, and not an effect on actin polymerization in general.

We conducted additional experiments to test the validity of the actin expression system. To test the effect of exogenous actin expression on overall actin protein levels, we sorted transfected cells for low and high mCherry expression by flow cytometry, and then conducted western blot analysis for actin, mCherry and calnexin (loading control). None of the actin/mCherry vectors cause an increase in actin:calnexin ratio, in either the low- or high-

mCherry pools (SI Appendix Fig. S4A, B), suggesting that the level of exogenous actin is well below that of the total cellular actin pool.

Next, we assessed the possibility that expression of actin mutants changes overall actin filament distribution, by analyzing fixed cells stained with FITC-phalloidin. Visual examination of either the basal region or a medial region show no major differences in FITC staining between transfected and un-transfected cells for any of the constructs (SI Appendix Fig. S4C). We also examined the levels of GFP-F-tractin and mCherry expressed in the cells used for live-cell analysis of ionomycin response. None of the constructs displayed aberrantly high expression of F-tractin or mCherry (SI Appendix Fig. S4D,E), suggesting that effects of the K50Q and K61Q constructs are not due to over-expression of these constructs. In fact, the levels of mCherry expression in the K50Q mutant-expressing cells were consistently lower than in the other samples. Finally, we examined the effect of F-tractin expression level on the ionomycin-induced actin burst response, and found a linear relationship between initial F-tractin intensity and peak ionomycin-induced F-tractin intensity (SI Appendix Fig. S4F). Since F-tractin levels are similar between the constructs tested, this result shows that the system is not saturated for F-tractin.

Our overall conclusion is that two actin mutants, K50Q and K61Q, significantly compromise INF2 activation in U2OS cells. In contrast, K328Q has little effect on INF2 activation.

Direct binding studies suggest that CAP-WH2 domain binds INF2-DID, while CAP/Ac-actin binds INF2-DAD

We used fluorescence anisotropy to examine binding between the WH2 motifs of CAP1 or CAP2 (SI Appendix Fig. S5A) with both WT and K50Q β-actin monomers, as well as with INF2's DID-containing N-terminal region. In parallel, we conducted similar binding studies for INF2's DAD-containing C-terminal region. A schematic of the interactions tested here is in Figure 5A.

Similar to past results using muscle actin (6, 7), INF2-Cterm binds both WT-actin and K50Q-actin with K_d^{app} of 78 nM and 63 nM, respectively (Fig. 5B). In contrast, neither CAP1-WH2 nor CAP2-WH2 bind RSK-actin or WT-actin with sufficient affinity to determine an accurate dissociation constant, with estimated K_d^{app} of 10, 16, 25, and 22 μM respectively (Fig. 5C, SI Appendix Fig. S5B). Interestingly, the WH2 motifs from both CAP proteins display no detectable binding to K50Q-actin (Fig. 5C, SI Appendix Fig. S5B).

We previously showed that INF2-Cterm displays moderate affinity for CAP/actin (8). To test whether actin acetylation affects this interaction, we conducted anisotropy experiments for INF2-Cterm with either CAP/WT-actin or CAP/K50Q-actin. Interestingly, the affinity increases ~5-fold with K50Q-actin (Fig. 5D, K_d^{app} 1066 nM for CAP/WT-actin and 211 nM for CAP/K50Q-actin).

Finally, we tested the possibility that CAP-WH2 might interact with INF2-DID. Interestingly, both CAP1-WH2 and CAP2-WH2 display significant affinity for the N-terminal region of INF2 (Fig. 5E, SI Appendix Fig. S5C), with K_d^{app} of 480 nM and 390 nM, respectively. We have

previously shown that the A149D mutation in INF2-DID, which is analogous to a mutant that disrupts DID/DAD binding in mDia1, causes constitutive activation of INF2 in cells (6, 8). Interestingly, both CAP1-WH2 and CAP2-WH2 display reduced affinity for A149D-mutant INF2-DID (K_d^{app} of 1723 nM and 1148 nM, respectively). In contrast, INF2-Cterm displays low affinity for both WT- and A419D-INF2-Nterm (estimated K_d^{app} of 22 and 18 μM respectively, Fig. 5F), similar to previous findings (3).

CAP1 and CAP2 are present in excess over INF2 in U2OS cells

We used quantitative western blotting to determine levels of CAP1, CAP2 and INF2 in U2OS cells (SI Appendix Fig. 6). We first raised polyclonal antibodies against bacterially-expressed human CAP1 and CAP2, and determined the specificity of the antibodies against their respective CAP-GFP purified from HEK293 cells. Anti-CAP2 displays no observable cross-reactivity to CAP1 at the protein amounts tested, whereas anti-CAP1 displays weak CAP2 cross-reactivity, at ~30-fold less than CAP1 from band densities. Interestingly, the band of untagged CAP in both the CAP1-GFP and CAP2-GFP preparations appears to be predominately CAP1, since it is detected by anti-CAP1 but not anti-CAP2.

We determined a linear range of detection for purified CAP1-GFP, CAP2-GFP, and GFP-INF2-nonCAAX, using anti-INF2 raised previously (35) in the presence of fixed concentrations of U2OS cell extract. We then used U2OS extracts of well-defined cell and protein concentrations to analyze CAP1, CAP2, and INF2 signal intensity in the linear detection range. Both CAP1-GFP and CAP2-GFP display doublet bands by western, and we used both bands for quantification. From extracts, CAP2 runs as a doublet, and we used the lower band for quantification.

U20S cells contain $7.95x10^6$, $4.44x10^5$, and $8.79x10^4$ molecules/cell of CAP1, CAP2 and INF2, respectively (Table 1). From the same extract, the total actin concentration is $1.96x10^8$ molecules/cell (Table 1), similar to that determined previously (43). To estimate cytoplasmic concentrations, we used cell and organelle volumes determined from an in-depth lattice light sheet study of Cos7 cells (44), with the resulting cytoplasmic volume (3.14 pL) approximating that determined for NIH 3T3 cells (2.26 pL) using different methods (45). These estimates are provided in Table 1. Overall, CAP1 and CAP2 are approximately 90- and 5-fold more abundant than INF2 in U2OS cells.

Discussion

We make the following advances concerning the mechanism of INF2 regulation by CAP/KAc-actin. First, we show that acetyl-mimetic mutants of two residues, K50 and K61, confer inhibitory activity to β-actin when coupled to CAP, both in biochemical assays and in cells. Second, we provide evidence that the DID of INF2 does not engage in an autoinhibitory interaction with its DAD but binds the WH2 of CAP, while INF2-DAD binds at another site on the CAP/KAc-actin complex in a manner that is influenced by actin acetylation. These findings support a bridge model for INF2 inhibition (Figure 1D).

We purified recombinant β-actin as well as three mutants, K50Q, K61Q and K328Q, for biochemical assays. The positions of these three residues suggested that the mutations would not affect the basic polymerization properties of actin. Indeed, the critical concentrations of all β-actins made here appear similar to RSK-actin, while there are minor differences in polymerization kinetics. Most importantly, all of the mutant actins are efficiently polymerized by INF2, suggesting that acetylated actin alone is not an INF2 inhibitor.

When in complex with CAP2, two acetyl-mimetic mutants (K50Q and K61Q) inhibit INF2 with significantly higher potency than WT-actin. The inhibition potency of CAP2/K50Q-actin (IC_{50} of 212 nM) is comparable to that of the inhibitory CAP/actin complexes we identified previously (CAP2/brain actin and CAP2/chicken muscle actin, IC_{50}s of 54 and 254 nM, respectively). CAP2/K61Q-actin is not as potent, with an estimated IC50 of 772 nM. In contrast, CAP2/K328Q-actin displays negligible INF2 inhibitory activity.

These results suggest that acetylation in sub-domain 2 of the actin monomer is key to INF2 inhibition. K50 is in the "D-loop", which is unstructured in many actin structures, whereas K61 is in a helical region. Both residues face away from CAP in the CARP/actin crystal structure (Figure 1C). Intriguingly, this region of sub-domain 2 gets pulled back towards CARP (12), further exposing these residues (Figure 1C).

This study represents the first mechanistic evaluation of actin acetylation effects and, as such, raises interesting new questions. First, might dual acetylation of K50 and K61 increase INF2 inhibition, as suggested for K326 and K328 acetylation in *Drosophila* flight muscle (26)? Second, how does actin acetylation interface with other actin post-translational modifications? Interestingly, K50 and K61 reside near M44 and M47, which are substrates for MICAL-mediated oxidation (50). Third, do other acetylated lysines play roles in INF2 regulation? We had previously identified several other acetylated lysines (8), and a number of additional acetylation sites have been identified in proteomic screens (24).

As an aside, both INF2-full length and INF2-FFC do increase the apparent critical concentration slightly for all actins tested. This change might reflect INF2's severing/depolymerization ability (7, 36, 37), or the relative effects of the FH2 on on-rate and off-rate at the barbed end, which varies between formins (46-49). We have previously found that INF2-FFC slows barbed end elongation by ~60% (37).

Actin binding by full-length CAP reveals several interesting features. First, full-length CAP2 can bind ATP-actin with high affinity, since significant ATP-actin remains on CAP after extensive purification in nucleotide-free buffer. Given that previous results have shown the CARP domain to have much higher affinity for ADP-actin than for ATP-actin (11-13), this result is surprising, and suggests that the full-length protein varies somewhat. The WH2 motif is not to be the major ATP-actin binder, since it has low affinity ATP-actin (Figure 5). However, the situation might be different in the context of the full-length CAP. Second, full-length CAP2 can allow nucleotide exchange on the bound actin, without causing its release. Third, ATP-actin can replace bound actin on CAP2. In view of the fact that the 'mock' exchange reactions do not result in loss of actin from CAP2, this result presents interesting questions as to how the exchange takes place.

This paper also provides new insights into the relevant interactions regulating INF2 activity. Two pieces of evidence suggest that INF2-DAD is binding primarily to actin in the CAP/actin complex, in a manner that is enhanced by actin acetylation. First, INF2-Cterm binds actin monomers with much higher affinity than it binds INF2-DID. While INF2's DID/DAD interaction would be significantly enhanced by their presence in the same polypeptide, the high affinity of INF2-DAD for actin disfavors DID/DAD interaction even in the full-length protein (6). Second, INF2-Cterm binds CAP/K50Q-actin with 5-fold higher affinity than CAP/WT-actin. We propose that INF2-DAD binds actin in an analogous manner to established WH2/actin interactions (5). We also hypothesize that the acetylated actin residues are not part of the binding interface, but that their acetylation results in conformational changes that enhance WH2 binding. Given their relative affinities for DAD, free actin monomers would be expected to out-compete CAP/K50Q-actin. However, the high concentration of profilin in mammalian cells reduces free actin levels substantially.

Our data also suggest that the relevant interaction of INF2-DID is with CAP-WH2, based on the following data. First, both CAP1-WH2 and CAP2-WH2 bind the DID-containing INF2-Nterm with sub-micromolar affinity, which is appreciably tighter than INF2's own DID/DAD interaction. Second, neither WH2 motif binds actin monomers with appreciable affinity, and binding is undetectable to K50Q-actin. While it has been shown that actin monomer binding by the WH2 motif might be relevant for CAP's other biochemical functions (11-13), the lack of binding to K50Q-actin makes it unlikely to interact with actin in INF2 regulation.

Based on these results, we propose that CAP/KAc-actin inhibits INF2 by serving as a bridge between INF2-DID and INF2-DAD/WH2 (Figure 1D), rather than as a facilitator of INF2's DID/DAD interaction. KAc-actin is likely bound to CAP's CARP domain, since the HFD appears to only bind cofilin-bound actin monomers (15-18). One interesting structural feature is that CAP's CARP forms a back-to-back dimer, with actins on the outer surfaces (12), so that a 2:2 complex of CARP with KAc-actin might inhibit one INF2 dimer (8). Another interesting feature is that the N-terminal region of CAP has been shown to hexamerize (9, 10). Our previous studies suggested that both purified human CAP1 and CAP2 form hexameric complexes, raising the possibility that three INF2 dimers could be inhibited by one CAP hexamer bound to six acetylated actins. However, our fractionation results from mouse brain suggest that smaller

CAP-containing complexes might also exist (8), so the stoichiometry of the inhibitory complex in cells remains to be determined.

In our model, INF2 activation would occur through HDAC6-mediated de-acetylation of lysines in sub-domain 2, which would weaken the affinity of INF2-DAD for actin in the CAP/actin complex. Our proposal that the acetylated lysines do not form part of the DAD-binding interface would allow for HDAC6 access to the acetylated groups, resulting in the rapid stimulus-induced INF2 activation that we observe in cells (8, 41). The fate of the CAP/actin complex after deacetylation is interesting to consider. The complex could remain bound to INF2-DID, and influence INF2's activity on actin in a positive manner, possibly by directing ATP-bound actin monomers to FH1-bound profilin.

Our work here focuses on the INF2-nonCAAX splice variant, which is predominantly cytosolic. It is likely, however, that the ER-bound INF2-CAAX variant is subject to similar regulation because it is strongly inhibited in cells, similar to INF2-nonCAAX (6, 38, 40, 41). In addition, HDAC6 inhibition blocks the mitochondrial calcium increase that occurs downstream of both histamine and ionomycin stimulation in U2OS cells (8), an effect dependent upon INF2-CAAX (41).

Finally, we show that the cellular concentrations of CAP1 and CAP2 are in excess to that of INF2. These results suggest that CAP is in sufficient excess to inhibit INF2, in addition to its other cellular roles (14). CAP1 is nearly 20-fold more abundant than CAP2 in U2OS cells, so is likely the primary regulator of INF2 in this cell type. One question is how CAP's role in INF2 regulation is balanced with its other cellular roles. In addition, it will be important to determine the differential roles of CAP1 and CAP2 in INF2 regulation, as well as their own regulatory mechanisms. CAP1 has known phosphorylation sites just N-terminal to the CARP domain (51) that have been shown to influence its cellular effects, and CAP2 has sites that are possibly analogous. It is interesting that CAP2 consistently runs as a doublet, both from cell lysates and as the purified protein, possibly due to post-translational modification.

Materials and methods

Plasmids

Human INF2 full-length nonCAAX and CAP2 constructs described previously (8). For actin purification construct, the entire human wild type-β-actin-thymosin β4-6xHis tag cDNA (including stop codon 3' to 6xHis) was PCR amplified from an expression plasmid designed for insect cells (gift from Kathy Trybus) and subcloned into Xho1/EcoR1 sites of eGFP-N1 vector (Clonetech Inc). For bis-cistronic β-actin expression plasmid, human wildtype-β-actin alone was PCR amplified from the Trybus β-actin expression plasmid and cloned into Xho1/EcoR1 sites of PICherryNeo (Addgene #52119). For bacterial expression, CAP1 and CAP2 WH2 motifs (amino acid 247-292 and 254-297, respectively) were PCR amplified from human CAP1 and CAP2 cDNA (NovoPro 710829-5 (NM-006367) and 710470-11 (NM-006366)) and subcloned into BamH1/EcoR1 sites of pGEX-KT (52) with HRV3C protease site introduced between GST tag and WH2 motif. Human INF2-CAAX C-term (amino acids 941-1249) and DID-containing construct (amino acids 1-420) described previously (6). GFP-F-tractin plasmid described previously (41).

Protein expression, purification, and labeling

Rabbit skeletal muscle actin purified from acetone powder (53). Rabbit muscle actin labeled with pyrenyliodoacetamide (54). Both labeled and unlabeled actin gel-filtered on Superdex 75 16/60 (GE Biosciences) and stored in G-buffer (2 mM Tris-HCl pH 8, 0.5 mM DTT, 0.2 mM ATP, 0.1 mM $CaCl_2$, 0.01% w/v sodium azide) at 4°C. Expression and purification of INF2-FL non-CAAX, CAP1-GFP and CAP2-GFP in Expi 293-F cells (Life Tech #A14527) was described previously (8) and described in detail in the SI Appendix. For recombinant β-actin expression and purification in Expi 293-F cells, previously described methods (30, 31) were adapted, and are described in detail in the SI Appendix. Protein expression and purification of INF2-Nterm, INF2 C-term and the GST-fusion of human CAP1-Cterm from *E. coli* are described in (6) and (12). Labeling of INF2-Cterm with tetramethylrhodamine-succinimide (TMR, Molecular probes; C1171) previously described (6). Labeling of CAP1- and CAP2-WH2 with fluorescein isothiocyanate (FITC)-maleimide (Thermo Fisher; 62245) is described in the SI Appendix.

Antibodies

CAP1 and CAP2 rabbit polyclonal against GST-human CAP1 and GST-human CAP2 produced by Cocalico Biologicals Inc. Antibodies affinity purified using the GST-fusion proteins attached to Sulfo-link (ThermoFisher 20404) in presence of 10 mg/mL GST, and eluted in 200 mM glycine-HCl pH 1.9, then dialyzed into PBS. Anti-actin (mouse monoclonal, clone C4, Millipore, MAB1501), anti-calnexin (rabbit monoclonal， Cell Signaling, 2679), anti-mCherry (rat monoclonal, invitrogen, M11217). Anti-INF2 rabbit polyclonal was described previously (35). Secondary antibodies: IRDye 680RD goat anti-mouse (LiCor 926-68070), and IRDye 800CW goat anti-rabbit (LiCor 926-32211).

Actin biochemical assays

Pyrene actin polymerization assay and high-speed sedimentation assay are described in detail in the SI Appendix. Actin exchange onto CAP was described previously (8) and in the SI Appendix. Fluorescence anisotropy measurements were described in (6) and in detail in the SI Appendix. Units reported here are milli-anisotropy units. For CAP/actin nucleotide content

analysis**,** CAP2/293A was loaded on strep-tactin beads, then incubated in G-buffer alone (containing 0.2 mM ATP) or in G-buffer containing the indicated actin overnight at 4˚C with end-over-end rotation. Beads washed with 20CV G-buffer then 20 CV K50MEHD (10mM Hepes pH7.4, 50mM KCl, 1mM $MgCl_2$, 1mM EGTA, 1 mM DTT), before elution with K50MEHD containing 2.5mM dethiobiotin. Samples balanced for CAP2 protein mass by Coomassie-stained SDS-PAGE gel, then boiled 7min. Protein removed by centrifugation at 13,000xg 5 min and supernatant loaded onto 1mL SourceQ followed by salt gradient (0-150mM NaCl, 10mM Tris pH8.0) elution. Unexchanged samples were in K50MEHD, and were never exposed to ATP during purification or mock exchange.

Cellular assays

Live-cell and fixed-cell imaging methods are described in detail previously (41, 42) and in the SI Appendix. Flow cytometry is described in the SI Appendix. Quantification of CAP1, CAP2, INF2 and actin levels from U2OS cell extracts is described in detail in the SI Appendix. Cytosolic concentrations estimated using a cytoplasmic volume calculated for Cos7 cells obtained from (44), except for the nuclear volume which was provided by Sarah Cohen (University of North Carolina, Chapel Hill).

Statistical Analysis

Errors (standard error of the mean (except for table1, which was standard deviation)) were calculated using Excel (Microsoft, version 2007 or 2010). Binding curves were fit and dissociation constants (K_d) were calculated using KaleidaGraph 4.5.3. Linear standard curves were fit using Excel (Microsoft, version 2007 or 2010).

Data Availability

All data are available in the manuscript and supporting information.

Acknowledgements

We would like to thank Sarah Cohen for advice on nuclear volume in Cos7 cells, Roberto Dominguez for discussions and advice on WH2 motifs, Pekka Lappelainen for advice and C-terminal CAP protein, Nate Glurio for keeping us balanced, Dave Sept for his idea that CAP-WH2 might interact with INF2-DID, Chris Shoemaker for help with flow-sorting, and Kathy Trybus for help in establishing the actin expression/purification system. This work was supported by NIH R01 GM069818 and R35 GM122545 to HNH, R01 DK088826 to M. Pollak (HNH sub-contract), and P20 GM113132 to the BioMT COBRE.

Table 1

Concentrations of CAP1, CAP2, INF2 and actin in U2OS cells.

	Molecules/cell ($x10^6$)	**Cytoplasmic concentration (μM)**	**N**
CAP1	7.95 ± 1.23	4.21	8
CAP2	0.444 ± 0.089	0.24	6
INF2	0.0879 ± 0.0105	0.05	6
Actin	196 ± 12	104.00	6

Concentrations reflect CAP and INF2 monomers.

Figure Legends:

Fig. 1.

INF2, CAP, and the bridge model of INF2 inhibition. (A) Schematic of human INF2-nonCAAX (1,240 amino acids), including DID (amino acids 32-261), formin homology 1 domain (FH1, 421-520), formin homology 2 domain (FH2, 554-940), and DAD/WH2 (971-1000). Boundaries of the N-terminal construct (NT) and FH1-FH2-C (FFC) construct used in this study are also shown. (B) Schematic of human CAP2 (477 amino acids), including oligomerization domain (OD, amino acids 1-42), helical folded domain (HFD, 43-217), proline-rich region 1 (PP1, 229-245), WH2 motif (254-297), proline-rich region 2 (PP2, 308-323), and CARP domain (324-477). (C) Actin monomers (blue, gray surfaces) bound to dimeric CARP domain of CAP1 (black, green ribbons). K50, K61 and K328 on actin are highlighted in red, orange and yellow, respectively. Actin sub-domains indicated by white letters. N, amino-termini of CARP subunits. Adapted from PDB 6FM2. Bottom: structure rotated 90˚ to left. (D) Bridge model of INF2 inhibition by CAP/actin, whereby INF2-DID interacts with CAP-WH2, while INF2-DAD interacts with acetylated actin, which is bound to the CARP domain of CAP.

Fig. 2.

K-to-Q mutant actins are polymerization-competent. (A) Quantification of μM amounts of actin in supernatant from high-speed pelleting assays. Actins were polymerized 18 hr at 23˚C (2 μM actin), then ultra-centrifuged to separate polymerized actin (pellet) from monomeric actin (supernatant). Four conditions tested: actin alone (-), + 20 nM INF2-FL (FL), + 20 nM INF2-FFC (FFC), and + 10 nM capping protein (CP). Sample gels shown in Fig. S1C. (B) and (C) Pyrene-actin polymerization assays of 2 μM actin alone (B) or + 20 nM INF2-FL (C). Actin composition: 1.9 μM of the indicated actin + 0.1 μM pyrene-labeled RSK actin. (F) Time to half-maximum polymerization, measured from pyrene-actin curves similar to panels C-E.

Fig. 3.

β-actin mutants K50Q and K61Q, when bound to CAP2, inhibit INF2-mediated actin polymerization in biochemical assays. (A) Pyrene-actin polymerization assays (2 μM RSK-actin, 5% pyrene-labeled) containing 20 nM INF2-FL and 1 μM of the indicated CAP/actin complex. (B) Concentration curves of CAP/actin inhibition of INF2-FL polymerization activity, from assays similar to panel B. Polymerization activity of actin alone (black) and with INF2-FL (brown) shown to left of the curves. (C) Pyrene-actin polymerization assays of actin alone (2 μM RSK-actin, 5% pyrene-labeled) or in the presence of 1 μM of the indicated CAP/actin complex. (D) Pyrene-actin polymerization assays (2 μM RSK-actin, 5% pyrene-labeled) with 20 nM INF2-FFC and 1 μM of the indicated CAP/actin complex. (E) Pyrene-actin polymerization assays similar to those in panel D, in which varying ratios of K50Q:WT-b-actin were exchanged onto CAP2, then assayed for inhibition of INF2-FL. The percentages listed represent the percent K50Q-actin in the exchange reaction. Concentrations in pyrene-actin assays: 2 μM RSK-actin (5% pyrene), 20 nM INF2-FL, 1 μM CAP/actin. (F) Graph of INF2-FL activity in the presence of 1 μM CAP/actin as a function of % K50Q-actin in exchange reactions, from data similar to those in panel H.

Fig. 4.

β-actin K50Q and K61Q mutants inhibit the calcium-induced actin burst in U2OS cells. (A) Schematic of mammalian expression construct, co-expressing β-actin (un-tagged) and mCherry. (B) Micrographs of calcium-induced actin burst for cells expressing four β-actin constructs: WT, K61Q, K50Q and K328Q. U2OS cells were co-transfected with the β-actin/mCherry expression plasmid along with a plasmid containing GFP-Ftractin (to label actin filaments). Live cells were imaged for GFP and mCherry before and during stimulation with ionomycin (4 μM in serum-containing medium). Micrographs at left are full-field views of GFP and mCherry. Micrographs in center are zoomed views of GFP-Ftractin at three time points of ionomycin stimulation (0, 1 and 5 min) for two cells in the field: an mCherry-expressing cell (top) and a cell not expressing detectable mCherry (bottom). At right is a differential heat map showing the ratio of the actin signal at 1 min to the signal at 0 min (red/yellow colors denote higher 1min:0min ratio). Bars, 25 μm (left panels) and 10 μm (zooms). (C) Quantification of the ionomycin-induced actin burst for cells expressing WT β-actin, K50Q β-actin, K61Q β-actin, and K328Q β-actin, as compared to cells not expressing an actin/mCherry construct (untransfected). Results are from three experiments, with a total of 17 (untransfected), 38 (WT), 42 (K61Q), 29 (K50Q) and 34 (K328Q) cells analyzed. (G) Quantification of the CCCP-induced actin burst for cells transfected with the mCherry vector with no actin (Vector/CCCP, black, 61 cells), the mCherry/WT-actin vector (WT-actin/CCCP, green, 71 cells), or the mCherry/K50Q-actin vector (K50Q-actin/CCCP, red, 72 cells). Mock-stimulation of mCherry/no actin-transfected cells (Vector/DMSO, blue, 40 cells) shown for comparison. Results from 3 independent experiments.

Fig. 5.

CAP's WH2 binds INF2 DID, while INF2's DAD binds CAP/KAc-actin. (A) Schematic of binding interactions measured in the following panels, showing bars for INF2 (top bar) and CAP (bottom bars) and a purple square for actin. (B-F) Fluorescence anisotropy measurements using TAMRA-INF2-Cterm (50 nM) or FITC-CAP2-WH2 (100 nM). (B) Interaction between INF2-Cterm and WT-β-actin (black) or K50Q-β-actin (blue). (C) Interaction between CAP2-WH2 and RSK-actin (green), WT-β-actin (black) or K50Q-β-actin (blue). CAP1-WH2 results in SI Appendix S5B. (D) Interaction between INF2-Cterm and CAP/WT-β-actin (black) or CAP/K50Q-β-actin (blue) complex. (E) Interaction between CAP2-WH2 and INF2-Nterm (black) or INF2-A149D-Nterm (blue). CAP1-WH2 results in SI Appendix S5C. (F) Interaction between INF2-Cterm (right) and INF2-Nterm (black) or INF2-A149D-Nterm (blue). All anisotropy values in milli-anisotropy units.

1. Higgs HN (2005) Formin proteins: a domain-based approach. *Trends Biochem Sci* 30(6):342-353.
2. Goode BL & Eck MJ (2007) Mechanism and Function of Formins in Control of Actin Assembly. *Annu Rev Biochem*.
3. Sun H, Schlondorff JS, Brown EJ, Higgs HN, & Pollak MR (2011) Rho activation of mDia formins is modulated by an interaction with inverted formin 2 (INF2). *Proc Natl Acad Sci U S A* 108(7):2933-2938.
4. Li F & Higgs HN (2003) The mouse formin mDia1 is a potent actin nucleation factor regulated by autoinhibition. *Curr Biol* 13(15):1335-1340.
5. Dominguez R (2016) The WH2 Domain and Actin Nucleation: Necessary but Insufficient. *Trends Biochem Sci* 41(6):478-490.
6. Ramabhadran V, Hatch AL, & Higgs HN (2013) Actin monomers activate inverted formin 2 by competing with its autoinhibitory interaction. *J Biol Chem* 288(37):26847-26855.
7. Chhabra ES & Higgs HN (2006) INF2 Is a WASP homology 2 motif-containing formin that severs actin filaments and accelerates both polymerization and depolymerization. *J Biol Chem* 281(36):26754-26767.
8. A M, Fung TS, Kettenbach AN, Chakrabarti R, & Higgs HN (2019) A complex containing lysine-acetylated actin inhibits the formin INF2. *Nat Cell Biol* 21(5):592-602.
9. Jansen S, Collins A, Golden L, Sokolova O, & Goode BL (2014) Structure and mechanism of mouse cyclase-associated protein (CAP1) in regulating actin dynamics. *J Biol Chem* 289(44):30732-30742.
10. Chaudhry F*, et al.* (2013) Srv2/cyclase-associated protein forms hexameric shurikens that directly catalyze actin filament severing by cofilin. *Mol Biol Cell* 24(1):31-41.
11. Mattila PK*, et al.* (2004) A high-affinity interaction with ADP-actin monomers underlies the mechanism and in vivo function of Srv2/cyclase-associated protein. *Mol Biol Cell* 15(11):5158-5171.
12. Kotila T*, et al.* (2018) Structural basis of actin monomer re-charging by cyclase-associated protein. *Nat Commun* 9(1):1892.
13. Chaudhry F, Little K, Talarico L, Quintero-Monzon O, & Goode BL (2010) A central role for the WH2 domain of Srv2/CAP in recharging actin monomers to drive actin turnover in vitro and in vivo. *Cytoskeleton (Hoboken)* 67(2):120-133.
14. Ono S (2013) The role of cyclase-associated protein in regulating actin filament dynamics - more than a monomer-sequestration factor. *J Cell Sci* 126(Pt 15):3249-3258.
15. Kotila T WH, Enkavi G, Kogan K, Vattulainen I, Jégou A, Romet-Lemonne G, Lappalainen P. (2019) Mechanism of synergistic actin filament pointed end depolymerization by cyclase-associated protein and cofilin. *Nat Commun*.
16. Makkonen M, Bertling E, Chebotareva NA, Baum J, & Lappalainen P (2013) Mammalian and malaria parasite cyclase-associated proteins catalyze nucleotide exchange on G-actin through a conserved mechanism. *J Biol Chem* 288(2):984-994.
17. Moriyama K & Yahara I (2002) Human CAP1 is a key factor in the recycling of cofilin and actin for rapid actin turnover. *J Cell Sci* 115(Pt 8):1591-1601.

18. Quintero-Monzon O*, et al.* (2009) Reconstitution and dissection of the 600-kDa Srv2/CAP complex: roles for oligomerization and cofilin-actin binding in driving actin turnover. *J Biol Chem* 284(16):10923-10934.
19. Narita T, Weinert BT, & Choudhary C (2019) Functions and mechanisms of non-histone protein acetylation. *Nat Rev Mol Cell Biol* 20(3):156-174.
20. Allfrey VG, Faulkner R, & Mirsky AE (1964) Acetylation and Methylation of Histones and Their Possible Role in the Regulation of Rna Synthesis. *Proc Natl Acad Sci U S A* 51:786-794.
21. Zhang X*, et al.* (2007) HDAC6 modulates cell motility by altering the acetylation level of cortactin. *Mol Cell* 27(2):197-213.
22. Li X*, et al.* (2017) Histone deacetylase 6 regulates cytokinesis and erythrocyte enucleation through deacetylation of formin protein mDia2. *Haematologica* 102(6):984-994.
23. Palazzo A, Ackerman B, & Gundersen GG (2003) Cell biology: Tubulin acetylation and cell motility. *Nature* 421(6920):230.
24. Hornbeck PV*, et al.* (2015) PhosphoSitePlus, 2014: mutations, PTMs and recalibrations. *Nucleic Acids Res* 43(Database issue):D512-520.
25. Terman JR & Kashina A (2013) Post-translational modification and regulation of actin. *Curr Opin Cell Biol* 25(1):30-38.
26. Viswanathan MC, Blice-Baum AC, Schmidt W, Foster DB, & Cammarato A (2015) Pseudo-acetylation of K326 and K328 of actin disrupts Drosophila melanogaster indirect flight muscle structure and performance. *Front Physiol* 6:116.
27. Kim DH*, et al.* (2015) A dysregulated acetyl/SUMO switch of FXR promotes hepatic inflammation in obesity. *EMBO J* 34(2):184-199.
28. Heidinger-Pauli JM, Unal E, & Koshland D (2009) Distinct targets of the Eco1 acetyltransferase modulate cohesion in S phase and in response to DNA damage. *Mol Cell* 34(3):311-321.
29. Gorsky MK, Burnouf S, Dols J, Mandelkow E, & Partridge L (2016) Acetylation mimic of lysine 280 exacerbates human Tau neurotoxicity in vivo. *Sci Rep* 6:22685.
30. Noguchi TQ, Kanzaki N, Ueno H, Hirose K, & Uyeda TQ (2007) A novel system for expressing toxic actin mutants in Dictyostelium and purification and characterization of a dominant lethal yeast actin mutant. *J Biol Chem* 282(38):27721-27727.
31. Lu H, Fagnant PM, Bookwalter CS, Joel P, & Trybus KM (2015) Vascular disease-causing mutation R258C in ACTA2 disrupts actin dynamics and interaction with myosin. *Proc Natl Acad Sci U S A* 112(31):E4168-4177.
32. Harris ES & Higgs HN (2006) Biochemical analysis of mammalian formin effects on actin dynamics. *Methods Enzymol* 406:190-214.
33. Pollard TD & Cooper JA (1986) Actin and actin-binding proteins. A critical evaluation of mechanisms and functions. *Annu Rev Biochem* 55:987-1035.
34. Chhabra ES, Ramabhadran V, Gerber SA, & Higgs HN (2009) INF2 is an endoplasmic reticulum-associated formin protein. *J Cell Sci* 122(Pt 9):1430-1440.
35. Ramabhadran V, Korobova F, Rahme GJ, & Higgs HN (2011) Splice variant-specific cellular function of the formin INF2 in maintenance of Golgi architecture. *Molecular biology of the cell* 22(24):4822-4833.

36. Gurel PS*, et al.* (2014) INF2-mediated severing through actin filament encirclement and disruption. *Current biology : CB* 24(2):156-164.
37. Gurel PS*, et al.* (2015) Assembly and turnover of short actin filaments by the formin INF2 and profilin. *J Biol Chem* 290(37):22494-22506.
38. Wales P*, et al.* (2016) Calcium-mediated actin reset (CaAR) mediates acute cell adaptations. *Elife* 5.
39. Shao X, Li Q, Mogilner A, Bershadsky AD, & Shivashankar GV (2015) Mechanical stimulation induces formin-dependent assembly of a perinuclear actin rim. *Proc Natl Acad Sci U S A* 112(20):E2595-2601.
40. Ji WK, Hatch AL, Merrill RA, Strack S, & Higgs HN (2015) Actin filaments target the oligomeric maturation of the dynamin GTPase Drp1 to mitochondrial fission sites. *eLife* 4:e11553.
41. Chakrabarti R*, et al.* (2018) INF2-mediated actin polymerization at the ER stimulates mitochondrial calcium uptake, inner membrane constriction, and division. *J Cell Biol* 217(1):251-268.
42. Fung TS, Ji WK, Higgs HN, & Chakrabarti R (2019) Two distinct actin filament populations have effects on mitochondria, with differences in stimuli and assembly factors. *J Cell Sci* 132(18).
43. Hatch AL, Ji WK, Merrill RA, Strack S, & Higgs HN (2016) Actin filaments as dynamic reservoirs for Drp1 recruitment. *Mol Biol Cell* 27(20):3109-3121.
44. Valm AM*, et al.* (2017) Applying systems-level spectral imaging and analysis to reveal the organelle interactome. *Nature* 546(7656):162-167.
45. Nguyen MM*, et al.* (2014) gamma-tubulin controls neuronal microtubule polarity independently of Golgi outposts. *Molecular biology of the cell*.
46. Pring M, Evangelista M, Boone C, Yang C, & Zigmond SH (2003) Mechanism of formin-induced nucleation of actin filaments. *Biochemistry* 42(2):486-496.
47. Kovar DR, Kuhn JR, Tichy AL, & Pollard TD (2003) The fission yeast cytokinesis formin Cdc12p is a barbed end actin filament capping protein gated by profilin. *J Cell Biol* 161(5):875-887.
48. Kovar DR, Harris ES, Mahaffy R, Higgs HN, & Pollard TD (2006) Control of the assembly of ATP- and ADP-actin by formins and profilin. *Cell* 124(2):423-435.
49. Pernier J, Shekhar S, Jegou A, Guichard B, & Carlier MF (2016) Profilin Interaction with Actin Filament Barbed End Controls Dynamic Instability, Capping, Branching, and Motility. *Dev Cell* 36(2):201-214.
50. Alto LT & Terman JR (2018) MICALs. *Curr Biol* 28(9):R538-R541.
51. Zhou GL, Zhang H, Wu H, Ghai P, & Field J (2014) Phosphorylation of the cytoskeletal protein CAP1 controls its association with cofilin and actin. *J Cell Sci* 127(Pt 23):5052-5065.
52. Hakes DJ & Dixon JE (1992) New vectors for high level expression of recombinant proteins in bacteria. *Analytical Biochemistry* 202(2):293-298.
53. Spudich JA & Watt S (1971) The regulation of rabbit skeletal muscle contraction. I. Biochemical studies of the interaction of the tropomyosin-troponin complex with actin and the proteolytic fragments of myosin. *J. Biol. Chem.* 246:4866-4871.

54. Cooper JA, Walker SB, & Pollard TD (1983) Pyrene actin: documentation of the validity of a sensitive assay for actin polymerization. *J Muscle Res Cell Motil* 4(2):253-262.
55. Nicholson-Dykstra SM & Higgs HN (2008) Arp2 depletion inhibits sheet-like protrusions but not linear protrusions of fibroblasts and lymphocytes. *Cell motility and the cytoskeleton* 65(11):904-922.

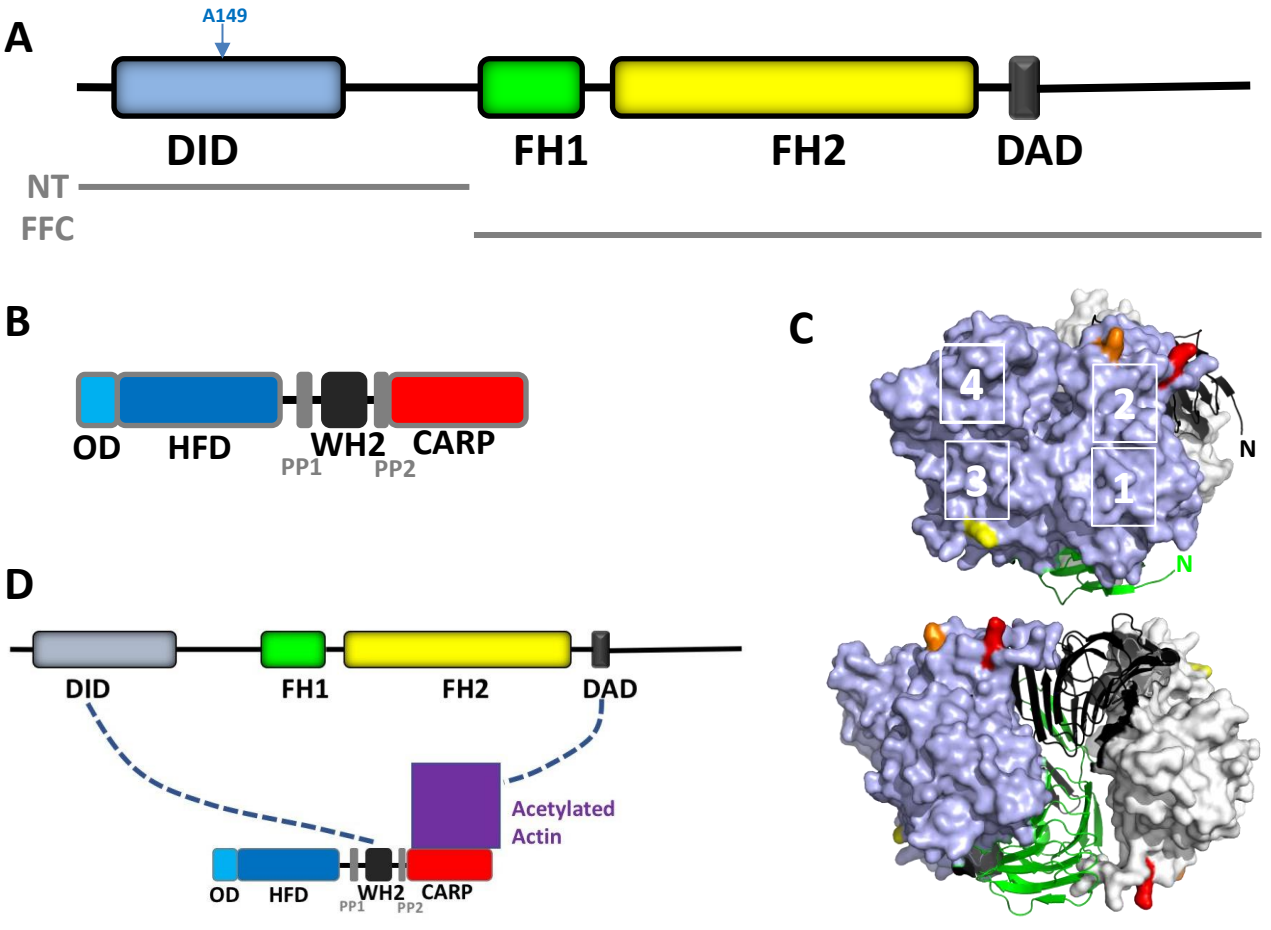
A
A149
DID
FH1
FH2
DAD
NT
FFC
B
OD
HFD
WH2
CARP
PP1
PP2
C
4
2
3
1
N
N
D
DID
FH1
FH2
DAD
Acetylated
Actin
OD
HFD
WH2
CARP
PP1
PP2

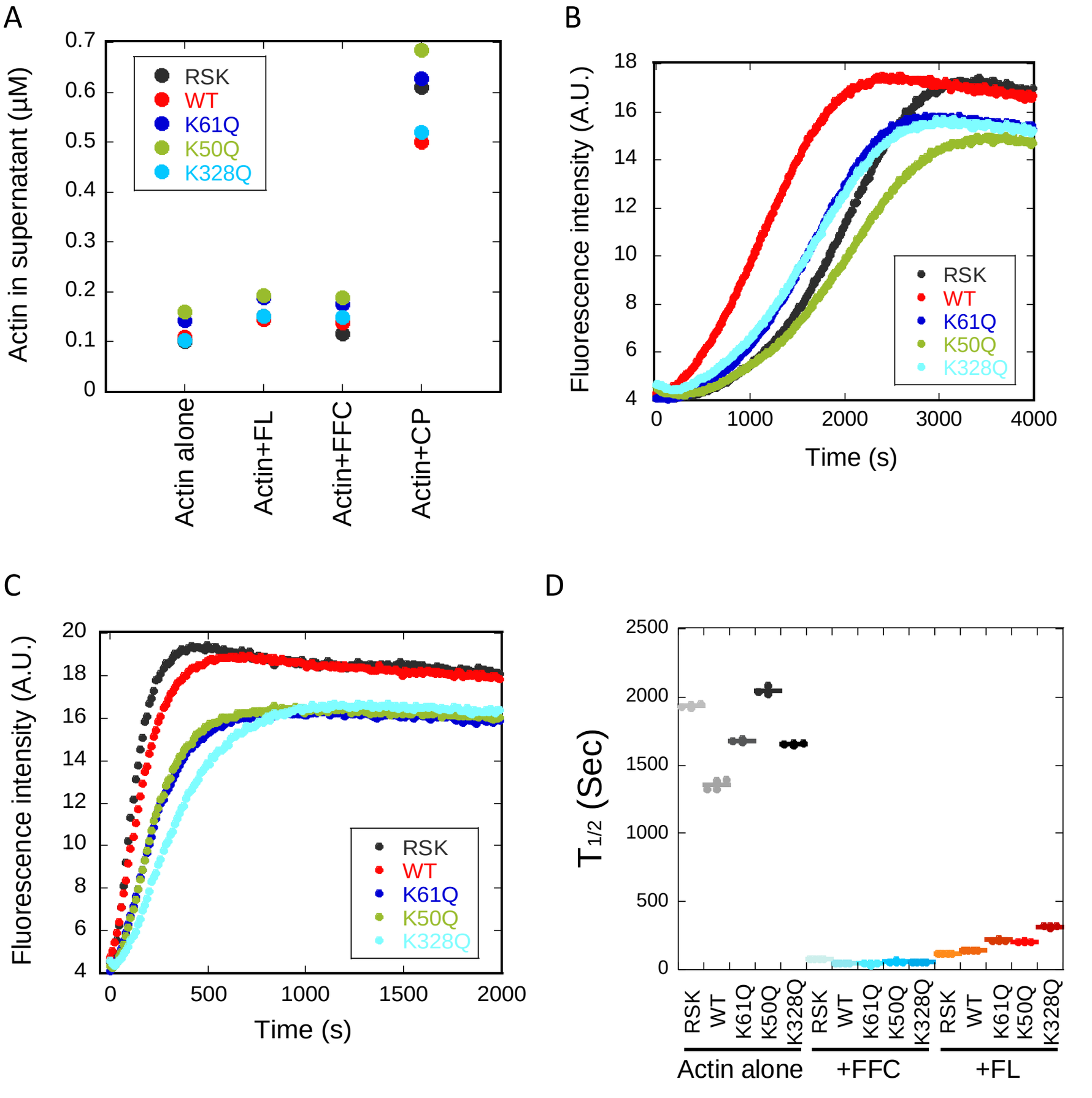
A
Actin in supernatant (μM)
0.7
0.6
0.5
0.4
0.3
0.2
0.1
0
RSK
WT
K61Q
K50Q
K328Q
Actin alone
Actin+FL
Actin+FFC
Actin+CP
B
Fluorescence intensity (A.U.)
18
16
14
12
10
8
6
4
0
1000
2000
3000
4000
Time (s)
RSK
WT
K61Q
K50Q
K328Q
C
Fluorescence intensity (A.U.)
20
18
16
14
12
10
8
6
4
0
500
1000
1500
2000
Time (s)
RSK
WT
K61Q
K50Q
K328Q
D
T1/2 (Sec)
2500
2000
1500
1000
500
0
RSK
WT
K61Q
K50Q
K328Q
RSK
WT
K61Q
K50Q
K328Q
RSK
WT
K61Q
K50Q
K328Q
Actin alone
+FFC
+FL

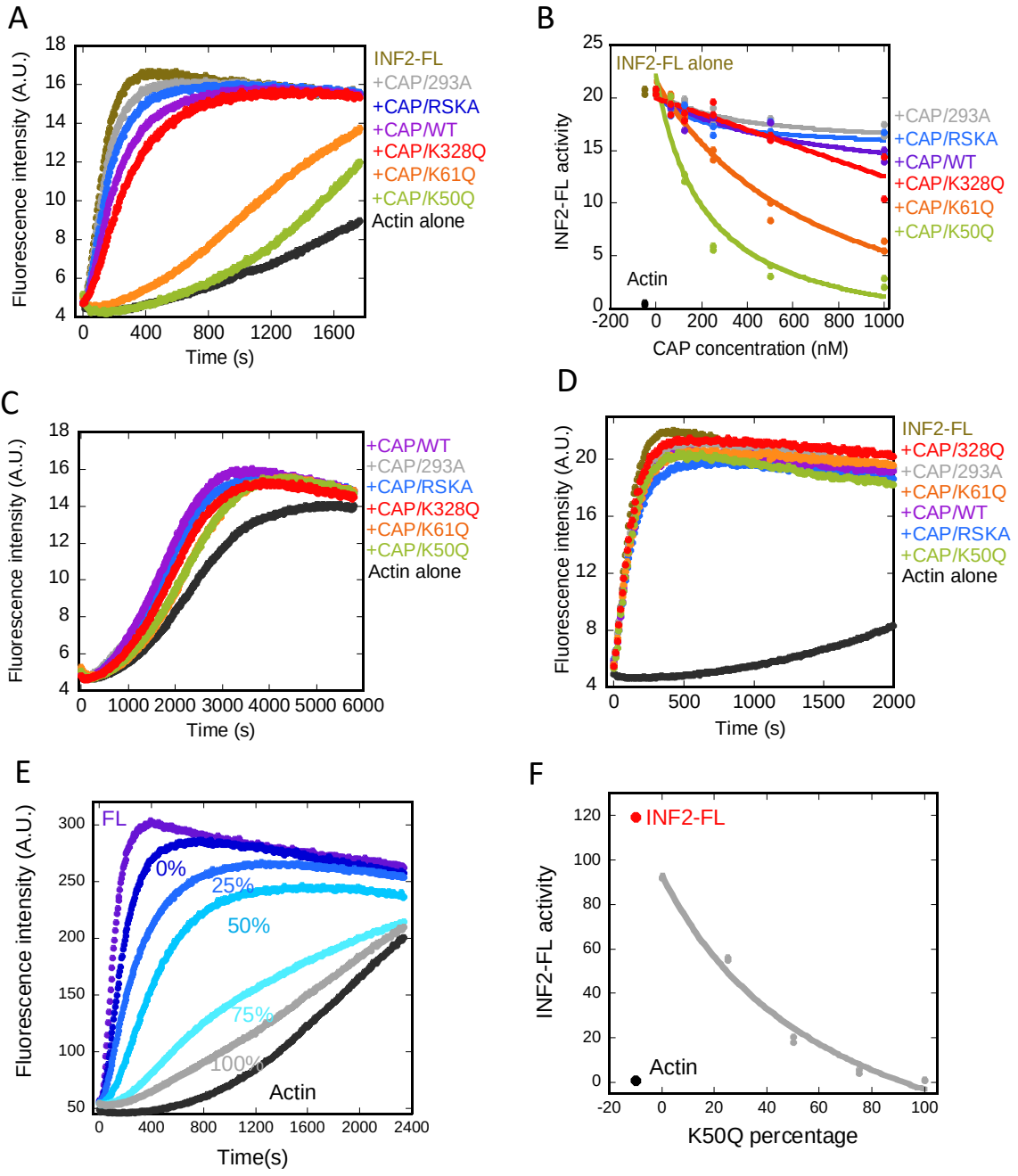
A
Fluorescence intensity (A.U.)
Time (s)
INF2-FL
+CAP/293A
+CAP/RSKA
+CAP/WT
+CAP/K328Q
+CAP/K61Q
+CAP/K50Q
Actin alone
B
INF2-FL alone
INF2-FL activity
CAP concentration (nM)
Actin
C
Fluorescence intensity (A.U.)
Time (s)
D
Fluorescence intensity (A.U.)
Time (s)
E
FL
0%
25%
50%
75%
100%
Actin
Fluorescence intensity (A.U.)
Time(s)
F
INF2-FL
INF2-FL activity
Actin
K50Q percentage

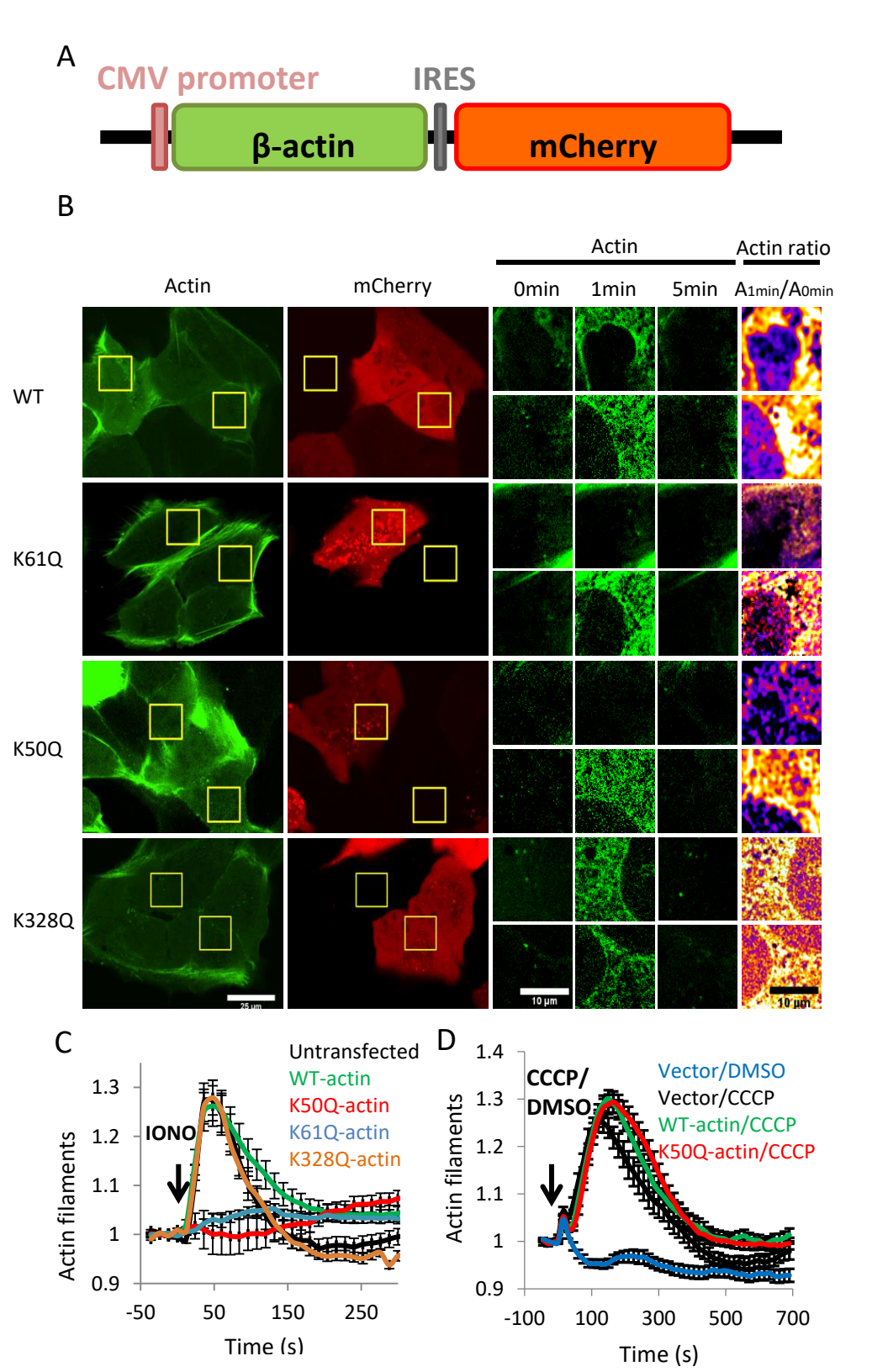
A
CMV promoter
IRES
β-actin
mCherry
B
Actin
Actin ratio
Actin
mCherry
0min
1min
5min
A1min/A0min
WT
K61Q
K50Q
K328Q
10 μm
C
Untransfected
WT-actin
K50Q-actin
K61Q-actin
K328Q-actin
IONO
Actin filaments
Time (s)
D
CCCP/
DMSO
Vector/DMSO
Vector/CCCP
WT-actin/CCCP
K50Q-actin/CCCP
Actin filaments
Time (s)

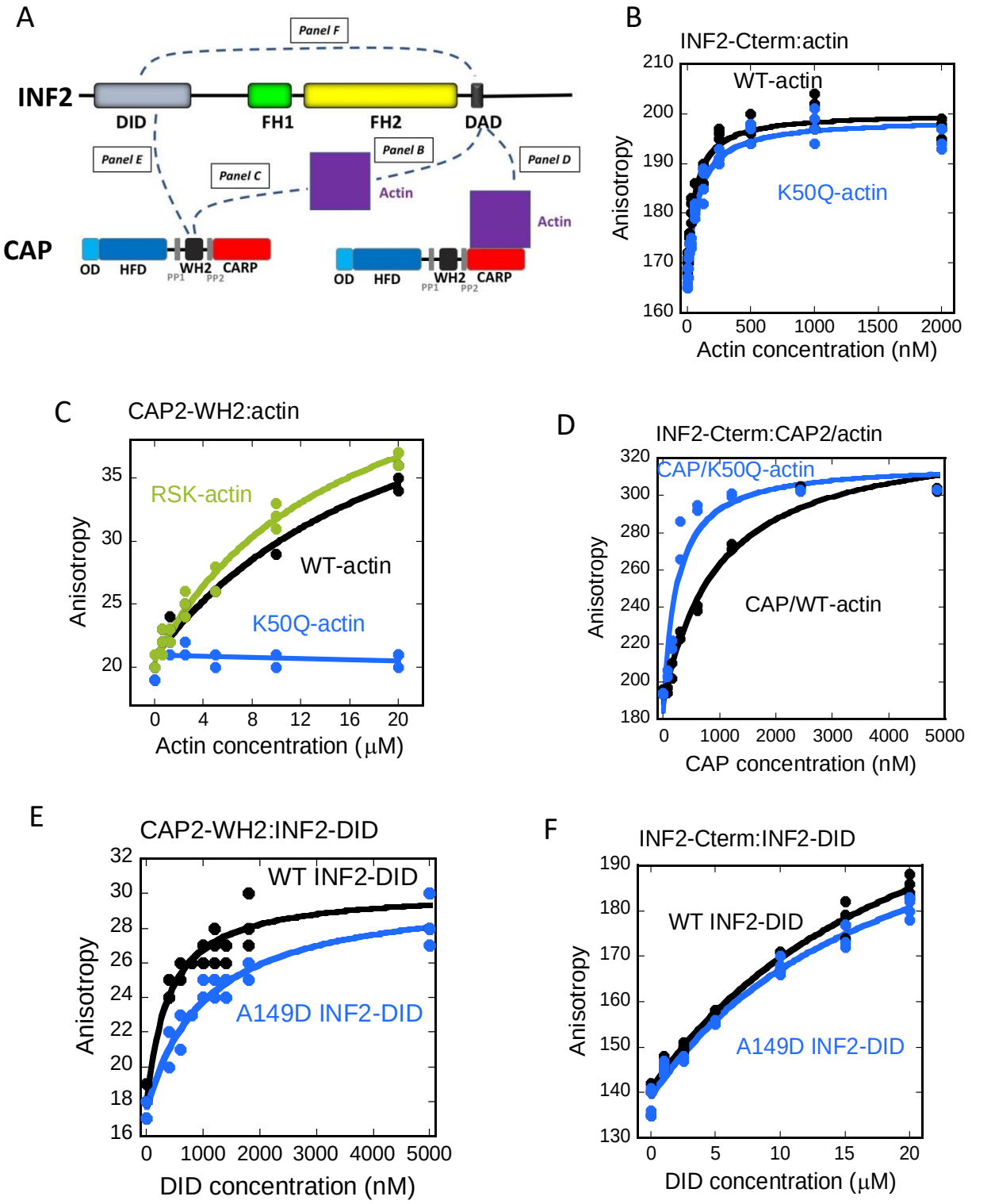
A
Panel F
INF2
DID
FH1
FH2
DAD
Panel E
Panel C
Panel B
Panel D
Actin
Actin
CAP
OD
HFD
WH2
CARP
PP1
PP2
OD
HFD
WH2
CARP
PP1
PP2
B
INF2-Cterm:actin
WT-actin
K50Q-actin
Anisotropy
Actin concentration (nM)
C
CAP2-WH2:actin
RSK-actin
WT-actin
K50Q-actin
Anisotropy
Actin concentration (μM)
D
INF2-Cterm:CAP2/actin
CAP/K50Q-actin
CAP/WT-actin
Anisotropy
CAP concentration (nM)
E
CAP2-WH2:INF2-DID
WT INF2-DID
A149D INF2-DID
Anisotropy
DID concentration (nM)
F
INF2-Cterm:INF2-DID
WT INF2-DID
A149D INF2-DID
Anisotropy
DID concentration (μM)

PNAS
www.pnas.org

Supplementary Information for

Regulation of INF2-mediated actin polymerization through site-specific lysine acetylation of actin itself

Mu A, Tak Shun Fung, Lisa M. Francomacaro, Thao Huynh, Tommi Kotila, Zdenek Svindrych & Henry N. Higgs

Corresponding Author: Henry N. Higgs
Email: henry.higgs@dartmouth.edu

This PDF file includes:

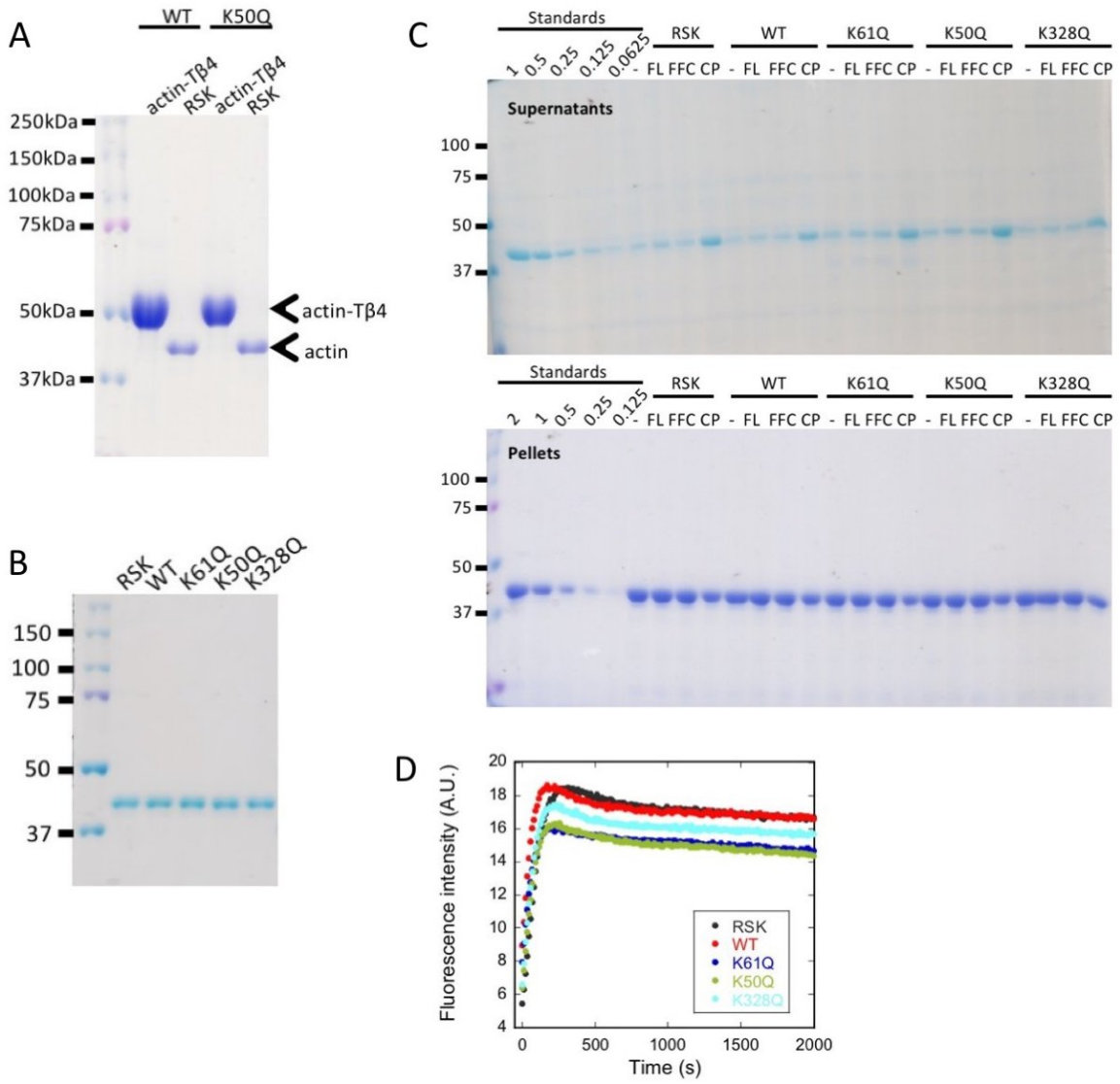

Fig. S1. Purified β-actin. (A) Coomassie gel of Ni-NTA eluted actin-Tβ4 construct, as well as rabbit muscle actin. (B) Coomassie-stained SDS-PAGE of purified β-actin (WT, K50Q, K61Q and K328Q), compared to rabbit muscle actin (RSK). 1 μg protein loaded on gel. (C) High-speed pelleting assays testing the polymerization of actin alone or with other proteins. Actin was polymerized 18 hr at 23˚C (2 μM actin), then ultra-centrifuged to separate polymerized actin (pellet) from monomeric actin (supernatant). Four conditions tested: actin alone (-), + 20 nM INF2-FL (FL), + 20 nM INF2-FFC (FFC), and + 10 nM capping protein (CP). Standards are RSK-actin corresponding to the indicated μM values under pelleting assay conditions. Gels loaded and stained differentially for supernatants and pellets, corresponding to higher actin levels in pellets under all conditions. (D) Pyrene-actin polymerization assays of 2 μM actin + 20 nM INF2-FFC. Actin composition: 1.9 μM of the indicated actin + 0.1 μM pyrene-labeled RSK actin.

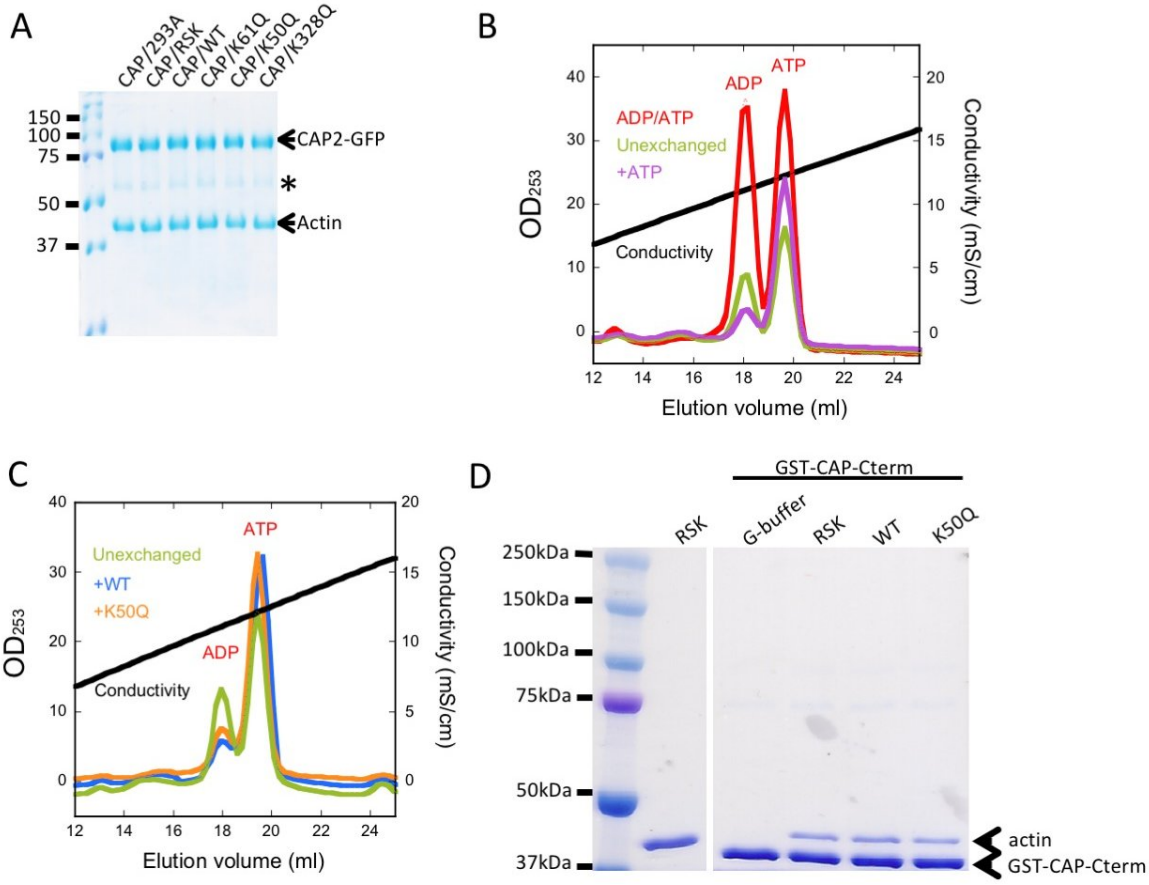

Fig. S2. CAP2/actin complex. (A) Coomassie-stained SDS-PAGE of purified CAP2/actin complexes after exchange with the indicated actins. CAP/293A represents mock-exchanged CAP that retains actin from HEK293 cell expression. 1 μg total protein loaded for each sample. Asterisk denotes untagged CAP (CAP1 from 293 cells, see Fig. S4A,B) that co-purifies with CAP2-GFP. (B) Nucleotide content of CAP2/293A, as judged by anion-exchange chromatography. Peaks of ATP and ADP standards shown in red (ADP/ATP). Purified CAP2/293A shown in green (unexchanged), and CAP2/293A that had been incubated overnight in 0.2 mM ATP shown in purple (+ATP). (C) Nucleotide content of CAP2/293A that has been subject to exchange with WT- or K50Q-□-actin. (D) Coomassie gel showing GST-CAP1-Cterm that has been incubated in G-buffer alone, or G-buffer containing a 5-mole excess of RSK-actin, WT- or K50Q-□-actin. Also shown is an RSK-actin standard at an amount that represents 50% of the expected signal if CAP is fully bound to actin in the experiment. The percentage of binding to CAP1-Cterm for the actins tested are: RSK, 14.6%; WT, 15.1%; K50Q, 13.8%. All lanes from the same gel and processed in the same manner, with intervening lanes cropped out.

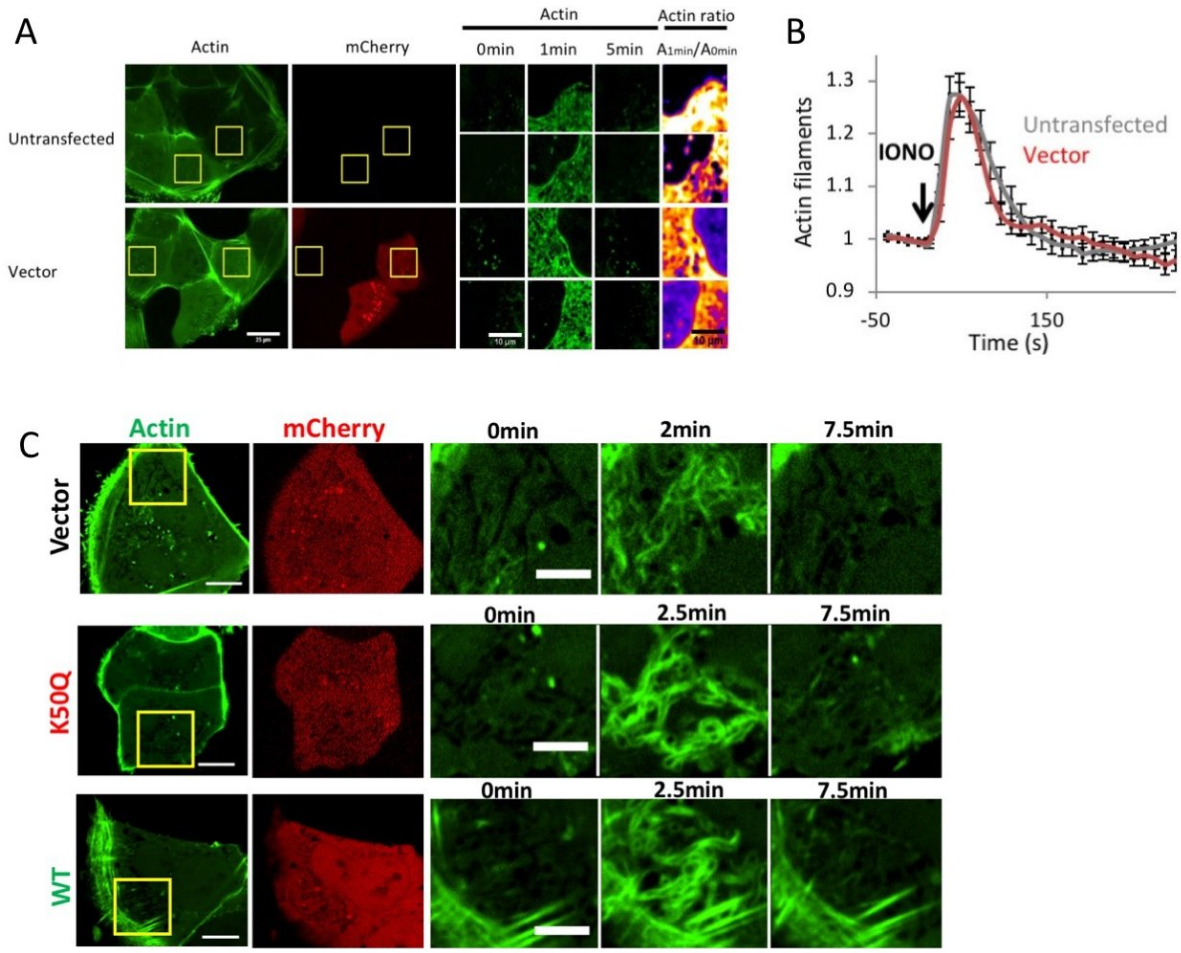

Fig. S3. Effects of b-actin in U2OS cells. (A) Micrographs of calcium-induced actin burst for cells not expressing mCherry (untransfected) or expressing the mCherry vector without an accompanying actin gene (Vector). Cells transfected with plasmid containing GFP-Ftractin (to label actin filaments) or co-transfected with this plasmid and plasmid expressing mCherry. Live cells imaged for GFP and mCherry before and during ionomycin stimulation (4 μM in serum-containing medium). Left: full-field views of GFP and mCherry. Center: zoomed views of GFP-Ftractin at three time points of ionomycin stimulation (0, 1 and 5 min) for two cells in the field: an mCherry-expressing cell (top) and a cell not expressing detectable mCherry (bottom). Right: differential heat map showing the ratio of the actin signal at 1 min to the signal at 0 min (red/yellow colors denote higher 1min:0min ratio). Bars, 25 μm (left panels) and 10 μm (zooms). (B) Graph quantifying the ionomycin-induced actin burst for untransfected or vector-expressing cells. Results from three experiments, total of 17 (untransfected) and 17 (Vector) cells analyzed. (C) Micrographs of CCCP-induced actin burst for cells expressing the mCherry vector without an accompanying actin gene (Vector), the mCherry/β-actin K50Q mutant (K50Q) or the mCherry/β-actin wild-type (WT) vector. U2OS cells co-transfected with a plasmid containing GFP-Ftractin and the plasmid expressing mCherry. Live cells imaged for GFP and mCherry before and during stimulation with CCCP (20 μM). Zoomed views of actin are shown before stimulation (0 min), at peak stimulation (2 or 2.5 min) and after depolymerization (7.5 min). Bars, 10 μm (left) and 5 μm (right).

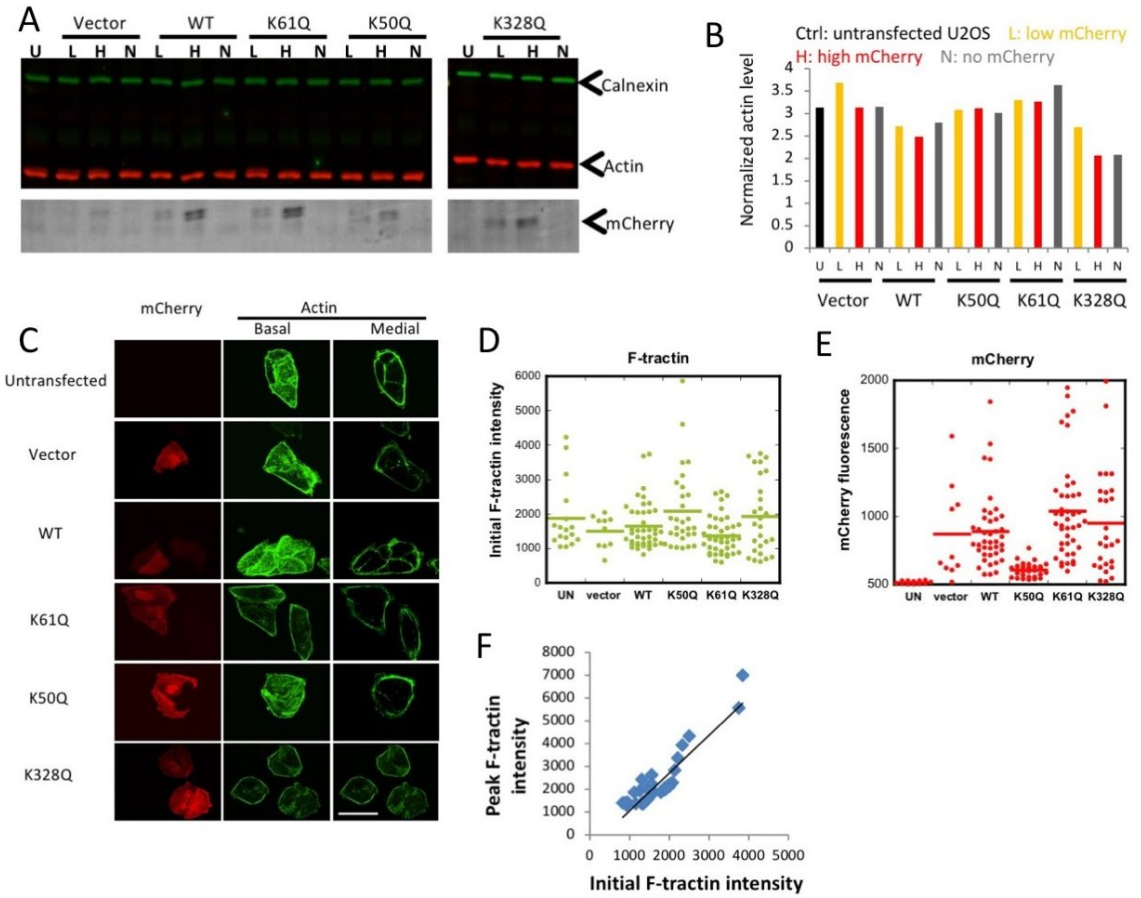

Fig. S4. Assessing effects of exogenously expressed β-actin. (A) Western blots of flow-sorted U2OS cells transfected with four versions of β-actin/mCherry vector (Vector = no β-actin). Cells sorted by mCherry signal level (L = low mCherry, H = high mCherry, N = no mCherry signal). Westerns of equal cell numbers probed for mCherry, actin, and calnexin (loading control). U = untransfected control. K328Q western is a different blot from others. (B) Densitometric quantification of actin levels of blots in panel A, normalized to calnexin signal. (C) Cells transfected with plasmids indicated, then fixed and stained with FITC-phalloidin. Two z sections shown, one at the basal region, and one in the medial region. Scale bar, 50 μm. (D) Quantification of overall cellular GFP-F-tractin intensity from U2OS cells co-transfected with GFP-F-tractin plasmid and indicated actin/mCherry co-expression vector. Intensity measurements taken in medial section prior to ionomycin stimulation (same data set as Fig. 4). UN = untransfected with actin/mCherry vector. Lines represent mean intensities: 1874±982 for UN (n = 17 cells, standard deviation), 1498±471 for vector (n = 10), 1657±685 for WT (n = 41), 2090±1155 for K50Q (n = 29), 1379±535 for K61Q (n = 43), and 1945±1094 for K328Q (n = 27). (E) Quantification of overall cellular mCherry intensity from U2OS cells co-transfected with GFP-F-tractin plasmid and indicated actin/mCherry co-expression vector. UN = untransfected with actin/mCherry vector. Lines represent mean intensities: 516±8.86 for UN (n = 17 cells, standard deviation), 871±350 for vector (n = 10), 890±267 for WT (n = 41), 607±53.8 for K50Q (n = 29), 1042±356 for K61Q (n = 43), and 953±381 for K328Q (n = 27). (F) Plot of F-tractin intensity at peak ionomycin stimulation versus initial F-tractin intensity for cells co-transfected with GFP-F-tractin plasmid and WT-β-actin/mCherry co-expression plasmid. Intensity measurements taken in a medial cell section (same data set as Fig. 1).

A

```
CAP1        247 SYESASRSSLFAQINQGESITHALKHVSDDMKTHKNPALKAQSG  291
CAP2        254 EESSPSRSALFAQLNQGEAITKGLRHVTDDQKTYKNPSLRAQGG  297
WAVE2       430 PAVSDARSDLLSAIRQG----FQLRRVEEQREQEKRDVVGNDVA  470
WIP          26 KTEQAGRNALLSDISKG----KKLKKTVTNDRSAPILDKPKGAG   66
INF2        966 QEEVCVIDALLADIRKG----FQLRKTARGRGDTDGGSKAASMD 1006
WASP        424 LAPGGGRGALLDQIRQG----IQLNKTPGAPESSALQPPPQSSE  464
IRSp53      500 GLDDYGARSMSRNPFAH----VQLKPTVTNDRSAPLLS        534
Lmod        516 TPQRSAHENLMEAIR-GSS-IKQLKRVEVPEALR            547
mDia1      1168 GDETGVMDSLLEALQSG----AAFRRKRGPRQANRKAGCAVTSL 1208
```

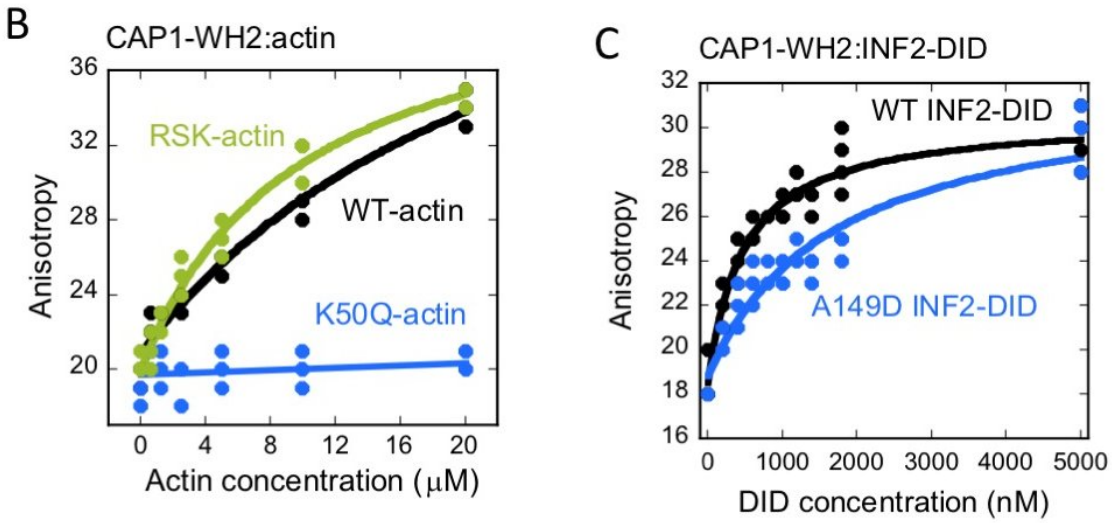

Fig. S5. Binding between CAP1 WH2 and actin or INF2-DID. (A) Alignment of WH2 regions for CAP1 and CAP2 with other WH2 motifs of or DAD sequences (all human sequences). Numbers indicate start and end amino acids. CAP sequences represent those used in binding studies, Red indicates positions of the 10 most conserved positions in WH2 motifs (1). (B) Interaction between CAP1-WH2 (100 nM) and RSK-actin (green), WT-β-actin (black) or K50Q-β-actin (blue) by fluorescence anisotropy. (C) Interaction between CAP1-WH2 and INF2-Nterm (black) or INF2-A149D-Nterm (blue) by fluorescence anisotropy. All anisotropy values in milli-anisotropy units.

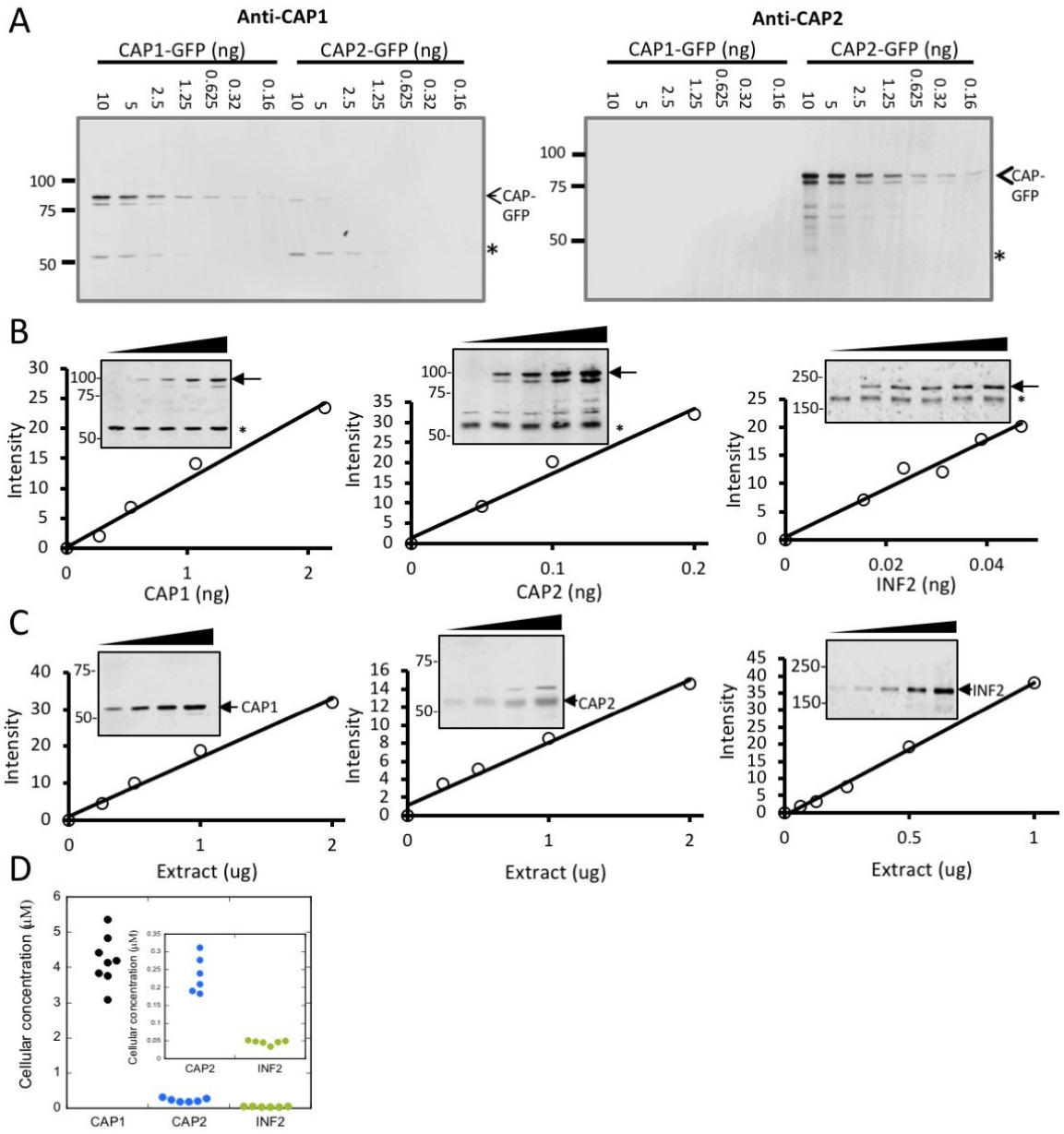

Fig. S6. CAP1, CAP2, INF2 and actin levels in U2OS cells. (A) Western blots of anti-CAP1 (left) and anti-CAP2 (right) against indicated ng amounts of purified GFP fusions. Arrows indicate GFP-CAP, asterisks indicate untagged CAP. (B) Quantification of western band intensity for anti-CAP1 (left), anti-CAP2 (middle), and anti-INF2 (right) against indicated ng amounts of purified CAP1-GFP, CAP2-GFP, or GFP-INF2-CAAX, respectively, mixed with 1 μg U2OS cell extract (CAP1, CAP2) or 0.5 μg U2OS cell extract (INF2). Arrows - CAP-GFP, asterisks - CAP from U2OS extract. Blots – dilution series of purified protein, corresponding to values on graph. (C) Quantification of western band intensity for indicated μg amounts of U2OS extract, blotted against anti-CAP1 (left), anti-CAP2 (middle), and anti-INF2 (right). Blots – dilution series of extract, corresponding to values on graph. (D) Dot plots of individual concentration determinations for CAP1, CAP2, and INF2. Inset - expanded Y-axis for CAP2 and INF2.

Supplementary Methods

Protein expression and purification

For protein expression in mammalian cells (INF2-FL non-CAAX, CAP1, CAP2, β-actin), 3 x 10^6 cells/mL Expi 293-F cells (Life Tech #A14527) growing in 1L Expi 293 expression medium (Life Tech A1435102) transfected with 1mg DNA and 3mg sterile 25kDa linear PEI mixed in Opti-MEM reduced-serum medium (Life Tech 31985070). 0.5mM enhancer 1 (Sigma # P4543) and 5mM enhancer 2 (Sigma # P1880) supplemented into the cell culture after 16hrs to boost protein expression. Proteins expressed at 37 °C, 8% CO_2 with shaking at 125 rpm for 2 days (INF2) or 3 days (CAP1, CAP2, β-actin).

For strep-tagged protein purification from Expi 293 cells, all steps were performed at 4°C or on ice. Cells pelleted at 300xg for 15min, and pellet resuspended in 45mL EB1 (100mM Hepes pH7.4, 500mM $NaCl_2$, 5mM EDTA, 1mM DTT, 1% v/v TritonX-100, protease inhibitors (2μg/mL leupeptin, 10μg/mL aprotinin, 2μg/mL pepstatin A, 1μg/mL calpeptin, 1μg/mL calpain inhibitor 1, 1mM bezamidine), 1:1000 dilution universal nuclease (ThermoFisher)) per 5mL pellet followed by 30min end-over-end incubation. Cell debris removed by ultracentrifugation at 185,000xg for 1 hr (Ti45 rotor, Beckman), and supernatant blocked with avidin (20μg/mL Sigma-Aldrich 189725) then applied to Strep-Tactin Superflow resin (2-1206-025; IBA, Göttingen, Germany) equilibrated in EB by gravity flow. After wash with WB (10mM Hepes pH7.4, 150mM $NaCl_2$, 1mM EDTA, 1mM DTT), column was either: 1) treated with HRV3C protease in WB (1:50 enzyme:substrate molar ratio) 16hrs at 4°C followed by 3 column volume WB wash; or 2) eluted with 10mM Hepes pH7.4, 150mM NaCl, 1mM EDTA, 1mM DTT, 2.5mM desthiobiotin. Protein concentrated with 30 kDa MWCO Amicon Ultra-15 (Millipore) before gel filtration through Superdex 200 16/60 (GE Bioscience) in 10mM Hepes pH7.4, 50mM KCl, 1mM $MgCl_2$, 1mM EGTA, 1mM DTT. Protein further concentrated to >10 μM before aliquoted, frozen in liquid nitrogen, and stored at -80˚C. N.B. – in all cases, Hepes pH given is pH at 23˚C.

For recombinant β-actin, all steps at 4°C or on ice. Cells pelleted at 300xg for 15min, and pellet resuspended in 45mL EB2 (1M Tris pH7.5 at 4C, 600mM NaCl, 0.5mM $MgCl_2$, 0.5mM Na_2ATP, 1mM DTT, 4% TritonX-100, 1mg/mL Tween, protease inhibitors, 1:1000 dilution universal nuclease) per 5mL pellet followed by 2hrs end-over-end incubation. Cell debris removed by ultracentrifugation at 185,000xg 1 hr (Ti45 rotor), and supernatant dialyzed into 10mM Hepes pH7.4 at RT, 0.25mM CaCl2, 300mM NaCl, 7mM β-ME. 0.05mM ATP then applied to Ni-NTA agarose resin (ThermoFisher #90115) by gravity flow. After wash with 10mM Hepes pH7.4 at RT, 0.25mM $CaCl_2$, 300mM NaCl, 7mM β-ME. 0.05mM ATP, 10mM imidazole, protein eluted with 10mM Hepes pH7.4 at RT, 0.25mM $CaCl_2$, 300mM NaCl, 7mM β-ME. 0.25mM ATP and 1ug/mL Leupeptin, 100mM imidazole to obtain β-actin-thymosinβ4-6xHis fusion. Protein dialyzed into G-buffer overnight and chymotrypsin digested (1:80-1:150 w/w chymotrypsin:actin, tested empirically for each preparation(Sigma C3142)) 1hr on ice. Reaction quenched by 2.5mM Diisopropylfluorophosphate, 2μg/mL leupeptin and 10μg/mL aprotinin. Cleaved full-length β-actin separated from other digestion products by SourceQ (GE Biosciences) eluting with 0-300 mM NaCl gradient (5mM Tris pH8.26 at 4C, 0.2mM CaCl2, 3mM NaN3. 0.5mM DTT, 1ug/mL leupeptin). 0.2mM ATP immediately added to SourceQ fractions, then dialyzed into 10mM Hepes pH7.4, 50mM KCl, 1mM $MgCl_2$, 1mM EGTA,

2 mM Tris-HCl pH 8, 0.5 mM DTT, 0.2 mM ATP, 0.1 mM $CaCl_2$, 0.01% w/v sodium azide overnight. Polymerized actin pelleted by ultracentrifugation 1 hr at 207,871xg, 4˚C (Ti70 rotor, Beckman) and resuspended with G-buffer. Filaments sheared through 27G needle, and dialyzed in G-buffer overnight. Depolymerized actin ultracentrifuged at 386,985xg (Ti70.1 rotor, Beckman) and supernatant gel-filtered on Superdex 75 16/60 (GE Biosciences) in G-buffer. Purified actin stored in G-buffer at 4°C under dialysis, changing buffer weekly.

For protein expression from *E. coli* (INF2-DID, INF2-Cterm, full-length CAP1, full-length CAP2, CAP1-WH2 and CAP2-WH2), Rosetta2 nonDE3 cells (Millipore/Sigma) transformed and grown at 37˚C in 1L Terrific Broth media containing 50µg/mL ampicillin and 34µg/mL chloramphenicol. 500µM IPTG added when OD_{600} reached 2, followed by overnight at 20˚C. All purification steps performed at 4°C or on ice. Cells pelleted at 600xg 15min, and pellet resuspended in 100mL EB3 (50 mM Tris pH 8, 500mM NaCl, 5mM EDTA, 1mM DTT, protease inhibitors, 1:1000 dilution universal nuclease) per 10g pellet. Cells disrupted using a Microfluidizer at 12000psi and debris removed by ultracentrifugation at 185,000xg for 1 hr (Ti45 rotor). Supernatant applied to Glutathione Sepharose resin (ThermoFisher #25236). After wash with 10 mM Tris-HCl pH 8, 250 mM NaCl, 1 mM EDTA, 1 mM DTT, 0.05% thesit, column was either: 1) treated with 0.5µM TEV protease in 10 mM Tris-HCl pH 8, 250 mM NaCl, 1 mM MgCl2, 1 mM EGTA, 1 mM DTT, 0.05% thesit overnight at 4°C to obtain untagged protein (INF2-Cterm); or 2) eluted with 10 mM Tris-HCl pH 8, 250 mM NaCl, 1 mM EDTA, 1 mM DTT, 0.05% thesit, 10mM reduced glutathione (CAP1, CAP2, CAP1-WH2 and CAP2-WH2). Protein gel filtered through Superdex 75 16/60 (GE Bioscience) in 10mM Hepes pH7.4, 50mM KCl, 1mM $MgCl_2$, 1mM EGTA, 1mM DTT.

For protein expression from *E. coli* of GST-fusions of CAP1-WH2 and CAP2-WH2 are, Rosetta2 nonDE3 cells (Millipore/Sigma) transformed and grown at 37˚C in 1L Terrific Broth media containing 50µg/mL ampicillin and 34µg/mL chloramphenicol. 500µM IPTG added when OD_{600} reached 2, followed by overnight at 20˚C. All purification steps performed at 4°C or on ice. Cells pelleted at 600xg 15min, and pellet resuspended in 100mL EB3 (50 mM Tris pH 8, 500mM NaCl, 5mM EDTA, 1mM DTT, protease inhibitors, 1:1000 dilution universal nuclease) per 10g pellet. Cells disrupted using a Microfluidizer at 12000psi and debris removed by ultracentrifugation at 185,000xg for 1 hr (Ti45 rotor). Supernatant applied to Glutathione Sepharose resin (ThermoFisher #25236). After wash with 10 mM Tris-HCl pH 8, 250 mM NaCl, 1 mM EDTA, 1 mM DTT, 0.05% thesit, column was either: 1) treated with 0.5µM TEV protease in 10 mM Tris-HCl pH 8, 250 mM NaCl, 1 mM MgCl2, 1 mM EGTA, 1 mM DTT, 0.05% thesit overnight at 4°C to obtain untagged protein (INF2-Cterm); or 2) eluted with 10 mM Tris-HCl pH 8, 250 mM NaCl, 1 mM EDTA, 1 mM DTT, 0.05% thesit, 10mM reduced glutathione (CAP1, CAP2, CAP1-WH2 and CAP2-WH2). Protein gel filtered through Superdex 75 16/60 (GE Bioscience) in 10mM Hepes pH7.4, 50mM KCl, 1mM $MgCl_2$, 1mM EGTA, 1mM DTT.

Protein labeling

Labeling of CAP1- and CAP2-WH2, GST-CAP1-WH2 and GST-CAP2-WH2 dialyzed into 20mM Hepes pH 7.4 at RT, 100mM KCl, 1mM TCEP at 4°C overnight, then incubated with 20-fold molar excess fluorescein isothiocyanate (FITC)-maleimide (Thermo Fisher;

62245) at 4°C overnight. Free dye removed by gel filtration using Superdex200 10/30 (GE Biosciences) in 10mM Hepes pH7.4, 50mM KCl, 1mM $MgCl_2$, 1mM EGTA, 1mM DTT. Protein reapplied to Glutathione Sepharose, then treated with HRV3C protease to elute the FITC-labeled WH2 peptide. The fragments containing HRV3C and 8xHis-tag were removed by passing eluted FITC-WH2 peptide through Ni-NTA. Final protein concentration determined by Bradford (BioRad) and FITC concentration using extinction coefficient 72,000 M^{-1} cm^{-1} at 495 nm. Calculated ratio of FITC:WH2 0.92 (CAP1-WH2) and 0.89 (CAP2-WH2).

Pyrene actin polymerization assay

Rabbit skeletal muscle actin or recombinant β-actin in G-buffer (6 μM actin, 5% pyrene) converted to Mg^{2+} salt by addition of EGTA and $MgCl_2$ (to 1 and 0.1 mM, respectively) for 2 min at 23°C immediately prior to polymerization. Polymerization induced by 2 volumes of 1.5xpolymerization buffer (75mM KCl, 1.5mM $MgCl_2$, 1.5mM EGTA, 15 mM Hepes pH 7.4, 2mM DTT, 2 mM Tris-HCl, 0.2 mM ATP, 0.1 mM$CaCl_2$, and 0.01% w/v NaN_3) containing other proteins. Pyrene fluorescence (365/410 nm) monitored in a 96-well fluorescence plate reader (Infinite M1000; Tecan, Mannedorf, Switzerland) within 1min of inducing polymerization. Slope of curve at ½ max is plotted to represent polymerization activity.

High-speed sedimentation assay

2 μM rabbit muscle actin or β-actin was polymerized alone, or with 20nM INF2-FL, 20nM INF2-FFC or 10nM capping protein in 1x polymerization buffer at room temperature overnight. Samples centrifuged at 80,000 rpm 20 min 4°C in TLA-100.1 rotor (Beckman). Supernatant carefully removed, pellets washed briefly and gently with polymerization buffer before resuspension in SDS-PAGE buffer. Samples resolved by SDS–PAGE. Gels stained either with Colloidal Blue Staining (Invitrogen LC6025) (supernatant) or Coomassie Blue Staining (BioRad 161-0400) (pellet), and band intensity analyzed using ImageJ software. Microgram amount of actin was quantified from rabbit muscle actin standards.

Actin exchange onto column-bound CAP

CAP2-GFP-2xstrep (also containing bound actin from 293 cells) was immobilized on strep-tactin beads (1 μM CAP2 monomer), then washed with G-buffer. The indicated species of actin (5 μM, in G-buffer) added and incubated with beads at 4°C with end-over-end rotation for 12hrs. Beads washed with 20 column volumes G-buffer. CAP2-GFP was removed from beads by either: eluting with G-buffer containing 2.5mM dethiobiotin, or 2) cleavage from beads by HRV3C protease (1:50, overnight at 4˚C). Concentration of CAP2-GFP was determined by densitometry (ImageJ) using actin as standards. For GST-CAP1-Cterm purified from *E. coli* (not containing bound actin) same procedure used with glutathione-sepharose resin and eluting with G-buffer containing 10mM reduced glutathione. Percentage of actin full binding was determined by densitometry (ImageJ) using RSK-actin as standard.

Fluorescence anisotropy

For measurements of CAP-WH2 or INF2-Cterm with actin monomer, fluorescent proteins diluted to 200 nM (fluorescein-labeled CAP1-WH2 or CAP2-WH2) or 100 nM (TMR-INF2-Cterm) in 2× polymerization buffer containing 0.02% thesit. Stock of actin

monomers mixed with 1.5× molar excess of latrunculin A (EMD Millipore, 428021) prepared in G-buffer, from which dilutions were further made. Equal volumes of FITC-CAP-WH2 and actin/LatA were incubated at least 1 hr in dark at 23˚C. For measurement of CAP-WH2 or INF2-Cterm with INF2-DID, fluorescent proteins diluted as above, and a stock of INF2-DID was prepared in 1xK50MEH/GT from which further dilutions were made. Equal volumes of FITC-CAP-WH2 and INF2-DID were mixed together and incubated overnight in dark at 23˚C before fluorescence readings. FITC fluorescence (470/525 nm) or TMR fluorescence (530/585 nm) anisotropy monitored in a 96-well fluorescence plate reader (Infinite M1000; Tecan, Mannedorf, Switzerland) and reported as milli-anisotropy units.

Quantification of protein cellular concentration

Quantitative western blotting was used to determine endogenous CAP1, CAP2, and INF2 concentration in U2OS cells, and Colloidal Blue Staining (Invitrogen LC6025) was used to determine endogenous actin concentration in U2OS cells. To prepare cell extract, cells growing logarithmically were trypsinized, washed in phosphate-buffered saline (PBS), then resuspended in PBS, and quantified for cell number (TC20, BioRad) and protein concentration (Bradford). Cellular protein was calculated at 0.37±0.045 ng/cell, similar to values obtained for other adherent cell types growing in monolayer (55). Protein extracted in 9 volumes of 4% SDS, 10 mM DTT followed by immediate boiling for 5 min, followed by 1 min in 23˚C water bath. *N*-ethylmaleimide (Sigma-Aldrich) added to 30 mM. Extract mixed 1:1 with 2xDB (250 mM Tris-HCl, pH 6.8, 2 mM EDTA, 20% glycerol, 0.8% SDS, 0.02% bromophenol blue, 1 M NaCl, 4 M urea) and further diluted with 1xDB to obtain desired concentrations. Linear concentration ranges determined for protein of interest for both the purified standard protein and the protein from extract. For the concentration determination by western (CAP1, CAP2 and INF2), purified GFP-fusion standard proteins were included as internal standards in fixed concentration of extract in the linear detection range. Proteins resolved by SDS–PAGE and detected by western blot using an Odyssey CLx Imager (Li-Cor). Band densities quantified using ImageJ (NIH). Both bands of the doublet CAP1-GFP and CAP2-GFP included in quantification. For actin, similar techniques were used as in past studies (43). Briefly, 4-10 μg total U2OS protein were compared with standard curve of RSK-actin (50-300 ng) by SDS-PAGE followed by colloidal Coomassie staining. Mean and standard deviation of eight (CAP1) or six (CAP2, INF2, actin) independent data points reported.

Cytosolic concentrations estimated using a cytoplasmic volume calculated for Cos7 cells by subtracting volumes of nucleus (0.902 pL), endoplasmic reticulum (1.538 pL), peroxisome (0.186 pL), mitochondria (0.179 pL), lysosome (0.089 pL) and Golgi (0.042 pL) from total cell volume (6.074 pL) obtained from (2), except for the nuclear volume which was provided by Sarah Cohen (University of North Carolina, Chapel Hill) from lattice lightsheet microscopy images. The cytoplasmic volume obtained (3.138 pL) is similar to that obtain previously for NIH 3T3 cells (2.26 pL) by different methods (55). Cytoplasmic concentrations should be taken as estimates for two reasons: 1) we do not have a cytoplasmic volume for U2OS cells; and 2) we have not determined whether the proteins examined here reside solely in cytoplasm.

Flow cytometry

U2OS cells co-expressing β-actin and mCherry were trypsinzed and washed into cold PBS. A Sony SH800 was used to sort untransfected cells (< 200 RFU), low mCherry expressing

cells (200-2000 RFU), and high mCherry expressing cells (>2000 RFU) using a 100 μm nozzle. Data collected using Sony Cell Sorter Software v 2.1.5. 20,000 cells collected for each condition and pelleted by centrifugation at 300xg for 5 min. Pellet washed with PBS then resuspended in 50 μL PBS. Cells were mixed 1:1 with 2xDB and analyzed by western blotting. Actin signal from each sample was normalized against calnexin signal.

Live cell imaging and analysis

Wild-type human osteosarcoma U2OS cells (American Type Culture Collection HTB96) grown in DMEM (Invitrogen) with 10% calf serum (Atlanta Biologicals). Cells tested every 6 months for mycoplasma using LookOut PCR detection kit (Sigma-Aldrich). Cells seeded at $4x10^5$ cells per well in 6-well dish ~16 hours prior to transfection. Plasmid transfections performed in OPTI-MEM media (Invitrogen) with 2 μL Lipofectamine 2000 (Invitrogen), 400 ng GFP-Ftractin, and/or 2 μg β-actin/mCherry per well for 6 hours, followed by trypsinization and re-plating onto glass bottom MatTek dishes (P35G-1.5-14-C) at ~$2x10^5$ cells per well. Cells imaged in DMEM (GIBCO, #21063-029 with 4.5g/L D-Glucose, L-Glutamine and 25Mm HEPES) supplemented with 10% NCS (HyClone, #SH30118.03) ~16-24 hours after transfection. Cells treated with 4 μM ionomycin (Sigma Aldrich I0634, from a 2 mM stock in DMSO), 20 μM Carbonyl cyanide 3-chlorophenylhydrazone (CCCP) (Sigma-Aldrich, C2759, from a 100 mM stock in DMSO), or same volume of DMSO (Invitrogen, D12345) at ~1 min after commencement of imaging, and imaging continued for 5-10 min (ionomycin) or 15~20min (CCCP) . Medium pre-equilibrated for temp and CO_2 content before use. Imaging conducted on a Dragonfly 302 spinning disk confocal (Andor Technology Inc, Belfast UK) on a Nikon Ti-E base and equipped with an iXon Ultra 888 EMCCD camera, and a Tokai Hit stage-top incubator. Lasers: solid state 405 smart diode 100 mW, solid state 488 OPSL smart laser 50 mW, solid state 560 OPSL smart laser 50 mW, solid state 637 OPSL smart laser 140 mW. Objective: 100x 1.4 NA CFI Plan Apo (Nikon). Images acquired using Fusion software (Andor). Imaging conducted in a medial region (approximately 2 μm above the basal surface) of cells expressing low level of mCherry,. Movies analyzed in blinded manner, with one individual coding movies, and another analyzing. Mean fluorescence calculated for each cell using ImageJ (NIH). Fluorescence values for each time point after drug treatment (F) were normalized by the average initial fluorescence (first 5-6 frames prior to stimulation-F0) and plotted against time as F/F0.

Fix cell imaging

Cells transfected with β-actin/mCherry and split onto MatTek dishes in same way as for live imaging. Cells fixed with 4% paraformaldehyde (Electron Microscopy Sciences Inc) in PBS 20min at 23˚C. After washing with PBS, cells permeabilized on ice with 0.25% Triton X-100 in PBS 15min. Cells washed with PBS prior to blocking with 10% calf serum in PBS for 1hr at 23˚C. Actin stained with 50 μg/mL FITC-phalloidin (Sigma-Aldrich) 1hr, and DNA stained with 0.1mg/L w/v DAPI (Calbiochem 268298) 10min at 23˚C in dark followed by PBS wash. Cells imaged in PBS using Dragonfly confocal with Zyla 4.2 Mpixel sCMOS camera, and z stacks with 0.2 μm stepsize taken. Images from ventral and medial z planes used.

References

1. Dominguez R (2016) The WH2 Domain and Actin Nucleation: Necessary but Insufficient. *Trends Biochem Sci* 41(6):478-490.
2. Valm AM*, et al.* (2017) Applying systems-level spectral imaging and analysis to reveal the organelle interactome. *Nature* 546(7656):162-167.